Electric Snowboard: The Glacier Glider

Submitted to Advisors
Professor William Michaelson
Professor Kenneth Stafford

By
James Englander
Nick Franzini
David Smith
Erin Thibeault

April 28, 2022

Abstract

The restriction of traditional snowboards to downhill terrain and the popularity of electric skateboards inspired the Glacier Glider, an electric snowboard capable of traversing over snowy flat ground and slight hills. The device is propelled with a tread system attached to adjustable suspension which accommodates different snow densities. Like an electric skateboard, the device is powered by a rechargeable battery and controlled with a handheld remote. A safety shield over the tracks also acts as a sled for downhill snowboarding.

Acknowledgements

The Electric Snowboard Team would like to thank our advisors Professor Stafford and Professor Michalson for their technical help and guidance. We would like to thank all the helpful people in Washburn including Professor Bergstrom, Nicholas Dal Porto, Hayden Furcolo, Thomas Sterrett and Chris Collins. We would also like to thank the Mechanical Engineering department, and specifically Barbara Furhman, for her assistance with acquiring materials. The team would like to thank the WPI Physics and Robotics departments for lending the team testing equipment. We would also like to thank Kevin Boenisch from Robosource Plastics and the anonymous man from craigslist for donating materials to the team. The Team would like to thank Mount Wachusett and Chris Stimpson for allowing us to test on their snow. We also would like to thank all those who have given us feedback at any point in our design process.

Thank you to friends, family and peers who took their time to offer feedback, attend presentations, and aid us in our design process. This project would not have been possible without your support.

Table of Contents

List of Figures

1.0 Introduction

Since snowboarding's conception in 1965, countless improvements have been made to the design of the snowboard to improve stability, maneuverability, and enjoyment. Improvements included forming the snowboard out of a single plank of wood and adding bindings to secure the rider's feet [1]. Around the same time, board sport enthusiasts started enjoying skateboarding during the offseason. The first commercially sold skateboard consisted of a narrow piece of wood, steel trucks and steel wheels, and has changed minimally since its conception [2]. The first motorized skateboard was invented in 1975 when Jim Rugroden created a two-stroke gasoline powered skateboard called the "MotoBoard" [3]. This skateboard was loud, dirty, and difficult to control, and was limited by the technology of its time. The design of the motorized skateboard has since improved; motorized skateboards today are cleaner, faster, and quieter, featuring electric motors, batteries, and wireless control. The invention of motorized skateboards expanded the capability of the skateboard, allowing for greater speeds, smoother rides, and an exciting new riding experience.

Snowboards, however, remain limited to riding down a sloped surface. Unlike on skis, no motion exists to propel the rider across flat terrain without unclipping from the device. For this reason, "cross-country snowboarding" has never existed. Unlike skateboards, there have been few successful improvements to expand the capability of a snowboard to replace manual pushing. In this Major Qualifying Project, the team designed and prototyped a single-person motorized board capable of traversing winter terrain for recreational use. The team built a propelled snowboard that combines the fun of recreational snowmobiling in a form factor more akin to a snowboard.

2.0 Background

Before an electric snowboard can be designed, the topics of traversing snow, initial models for motor and batteries, and the core components of the device must be understood. Beginning with traveling over snow, the main considerations for effective travel are flotation and ability to gain traction. To note, the term "flotation" is a misnomer; the true mechanism behind sinkage in snow is related to the snow's resistance to compaction and the contact pressure exerted on its surface, not buoyancy forces of a fluid. In this proposal, the term flotation will be used to describe an object's resistance to sinkage based on snow compaction. Then, the snow environment is incorporated into calculations to determine the minimum required torque and power to drive the entire system. Following that are relevant devices which provide insight into design decisions made by previous teams to produce a working product or prototype. Finally, the key components, a battery, motor, electronic speed controller and user interface, are discussed to define needs and potential challenges.

2.1 Physics and Challenges of Traversing Over Snow

When traversing over snow, additional challenges are encountered, including: the tendency of a vehicle to sink, difficulty in achieving drive mechanism tractive force, and snow buildup in mechanical components. These difficulties influence design guidance based on a mixture of empirical evidence and the study of terramechanics. For a successful snow vehicle to achieve mobility, the vehicle must possess a sufficient surface-area-to-weight ratio to avoid excessive sinking, a sufficient traction and tractive effort to achieve thrust in various snow conditions, and successfully manage snow accumulation in core drive components [4] [5].

2.1.1 Surface Area Required for Flotation

Sinkage in snow is described by the amount of pressure exerted on the terrain surface by the contact area of the vehicle. The amount of sinkage of a snow vehicle is commonly measured experimentally because of the ground interface geometry, contact pressure and material properties of the terrain using model loading tests. Additionally, sinkage can be predicted with calculations from Terramechanics literature [4] [5], as found in *Equation 2.1.2b*. Without performing experiments or estimating snow properties required for *Equation 2.1.2b*, a reasonable estimate for the required surface area can be acquired from current devices. Snowshoes, for example, are designed to support a given weight according to their total surface area. A ratio of carrying weight to total surface area can then be found to approximate the maximum pressure exerted on the snow by snowshoes. Using a snowshoe manufacturer's weight limits for various sizes, the average contact pressure of snowshoes was found to be 3,300 Pa, the full calculation of which is detailed in *Appendix 6.A.* Moreover, prior research suggested that the maximum recommended pressure of snow devices is between 3,000 and 5,000 Pa for small vehicles [6] [7]. With knowledge of a maximum pressure limit to avoid excessive sinking, a minimum surface area for over-snow devices can be estimated, as found in Section 3.2.1.

2.1.2 Tractive Force

The second major consideration in snow vehicle design is the tractive force to achieve thrust in given snow conditions. Unlike hard ground, motion on soft terrain relies heavily on the terrain's resistance to shearing to achieve traction. The tractive force (F_s) is developed from the interaction of the grousers and the terrain, as shown in *Figure 2.1.2.1*.

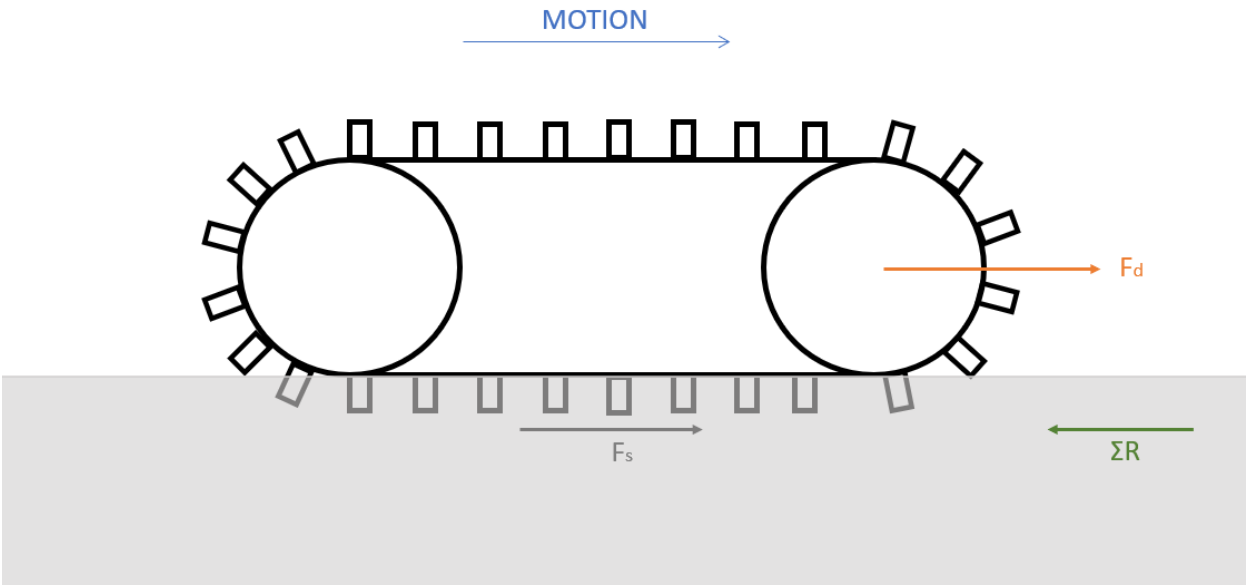

Fig 2.1.2.1 - Force balance of tracked vehicle on soft terrain.

For vehicles to gain traction on snow, the wheels or track must overcome all resistance to motion. The required tractive force a vehicle must produce must be greater than all the resistances associated with its motion to propel the vehicle forward. The total forward driving force produced by a vehicle in soft terrain, therefore, is limited by the accumulation of motion resistances that act opposite to vehicle motion. The net forward driving force that can be used for pulling or pushing a load after overcoming motion resistances is called "drawbar pull", the equation of which is defined in *Equation 2.1.2a* [8].

$$F_d = Fs - \Sigma R_f \qquad (2.1.2a)$$

Where ΣR_f is the sum of resistive forces that inhibit motion, F_d is the net forward force produced by the vehicle, and F_s is the total tractive force the vehicle can supply on a given terrain. As a vehicle moves through soft terrain, two main forms of resistance are encountered: compaction resistance and bulldozing resistance [4]. If a vehicle possesses any sliding surfaces, a sliding frictional resistance should also be incorporated. If the vehicle is on a hill, an additional resistance must also be included to account for gravity. Air resistance and other resistances can also be included but are negligible in this analysis. Air resistance was found to be minimal, causing an increase in required torque of only 1.6%. Internal resistance is also excluded here, as internal losses will be accounted for during motor selection and drive system design to achieve the desired drawbar pull. Using the contact pressure derived in Section 2.1.1, it is assumed adequate flotation can be achieved such that bulldozing resistance can be ignored. The remaining resistances used in preliminary calculations will be described here [5].

2.1.2.1 Compaction Resistance

Tracked Vehicles

Compaction resistance is related to vehicle sinkage and the force required to compact the terrain during motion. Using Bekker's *Equation 2.1.2b* for the pressure-sinkage relationship [5], the vehicle sinkage can be found.

$$z_0 = (\frac{p}{k_c/b + k_\phi})^{1/n} \tag{2.1.2b}$$

z_0 is the vehicle sinkage, p is the contact pressure, and k_c, $k\phi$ and n are empirical terrain parameters. Lastly, b represents the width of the contact patch that interacts with the terrain which, in treads, is equal to the total width of the track. This equation applies to tracked vehicles possessing a uniform contact pressure over the contact area.

Wong used Bekker's sinkage equation to derive the motion resistance known as compaction resistance. The compaction resistance represents the driving effort spent in compacting the terrain in front of a snow vehicle during its motion, which acts opposite to the direction of overall vehicle motion. Wong proposed that if a track is pulled a distance l, the work done by the towing force, which is equal to the compaction resistance force, is equated to the vertical work done in making a rut of length l. This compaction resistance R_c is shown in *Figure 2.1.2.2*, adapted from Bekker:

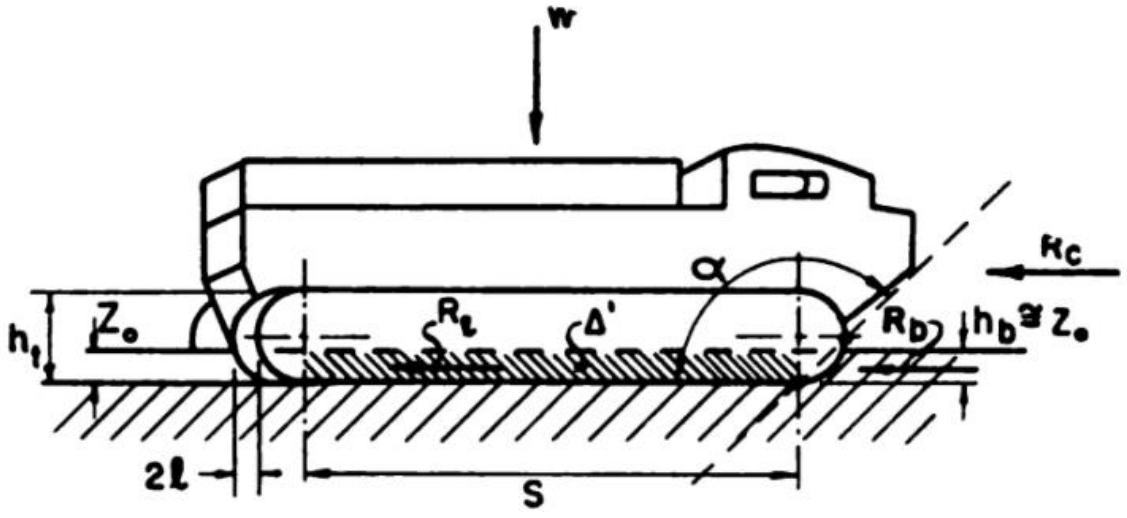

Figure 2.1.2.2 - Motion resistance due to compacting of the terrain, R_c acts opposite to overall vehicle motion [5].

The result of Wong's derivation is *Equation 2.1.2c*.

$$R_c = \frac{1}{(n+1)b^{1/n}(k_c/b + k_\phi)^{(1/n)}} (\frac{W}{l})^{(n+1)/n} \tag{2.1.2c}$$

This resistance is included as a force in the analysis in Section 3.1.

Wheeled Vehicles

Compaction resistance in wheeled tire drive systems is derived differently than in tracks. The compaction resistance of a rigid wheel on snow is shown in *Equation 2.2.2d* [9]:

$$R_c = \frac{bk}{n+1}\left[\frac{3W}{bk\sqrt{D}(3-n)}\right]^{\frac{2n+2}{2n+1}} \quad (2.2.2d)$$

Where *b* is the wheel width, *D* is the wheel diameter, *W* is the vertical load on the wheel, and *n* and *k* are empirical terrain parameters. This force again acts opposite to the direction of vehicle motion, thus requiring driving forces in excess to achieve mobility.

2.1.2.2 Sliding and Rolling Friction Resistance

If any sliding or rolling surfaces exist between the vehicle and the terrain, another resistive force must be included in analysis to represent contact friction. Frictional force is calculated based on the normal force between the vehicle contact area and the ground and the coefficient of friction between the two materials. This is shown in *Equation 2.2.2e*:

$$R_{fr} = \mu N \quad (2.2.2e)$$

If the vehicle is on a hill, only the portion of the vehicle weight that acts perpendicular to the riding surface is used as the normal force. The friction coefficient μ varies depending on the materials in contact, whether the contact area is sliding or rolling, and whether a static or kinetic model is considered. An estimate for μ between a waxed ski and snow of 0.1 is used in Section 2.2 for sliding friction, and 0.45 between rubber and snow is used for rolling friction [10] [11].

2.1.2.3 Tractive Force for Tracked Vehicles

In addition to motion resistances, a critical parameter to achieve mobility in snow is the tractive force F_p. For tracked vehicles, this force is called F_s, and its equation is known. The maximum tractive force $F_{s,\,max}$ that can be developed by a track is determined by the shear strength of the terrain τ_{max} and the contact area *A*, as shown in *Equation 2.1.2f*. The quantity τ_{max} can then be related to the terrain cohesion *c*, the vehicle weight *W* and the angle of internal shearing resistance φ in *Equation 2.1.2h*.

$$F_{s,max} = A\tau_{max} \quad (2.1.2f)$$

$$F_{s,max} = A(c + p\tan\phi) \quad (2.1.2g)$$

$$F_{s,max} = Ac + W\tan\phi \quad (2.1.2h)$$

The parameters φ and *c* are empirical terrain values found from shear tests. When the shear strength of the terrain is plotted against the normal pressure applied to its surface during shear tests, a straight line may be obtained [4] with shear strength on the y-axis and normal pressure on

the x-axis. The angle of this straight line relative to the horizontal represents the angle of internal shearing resistance φ, and the y-intercept represents terrain cohesion *c*. Examples of these graphs are shown below in *Figure 2.1.2.3*.

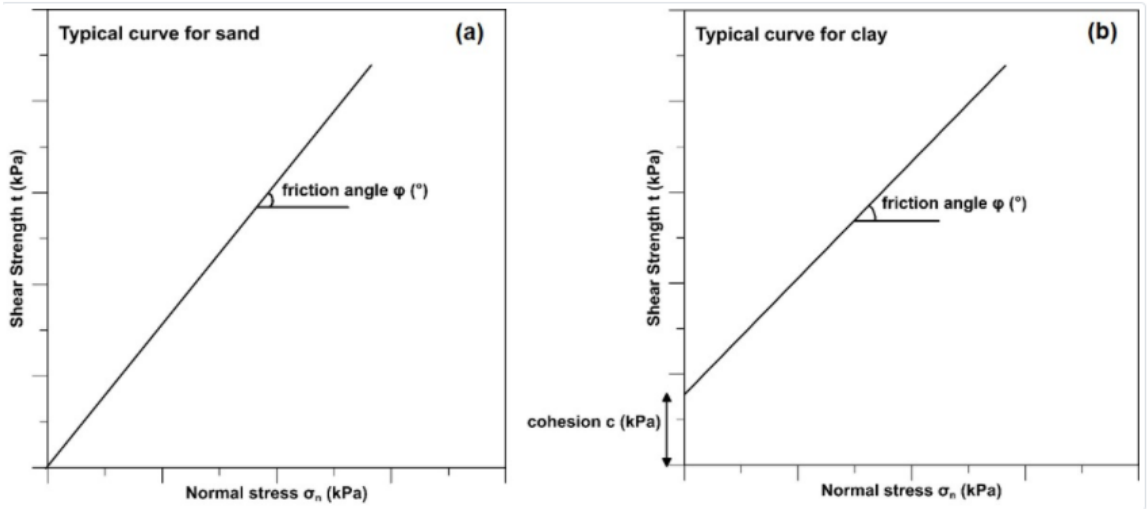

Figure 2.1.2.3 - Typical shear strength vs. normal pressure graphs of sand and clay [12].

The total tractive force a track can develop in real life is rarely the $F_{s,\,max}$ from *Equation 2.1.2h*. The tractive force a track develops in soft terrain is only a portion of $F_{s,\,max}$, which is determined by the amount of track slip. Methods for calculating track slip are based on a combination of terrain parameters and track geometry [4] [5] but can also be estimated when final track geometry and the variable snow parameters are not known using *Equation 2.1.2i*, where *S* is the loss coefficient due to track slip ranging from 0 to 1. If *S* is equal to 1, the track is assumed to have no slip, and F_s is equal to the full $F_{s,\,max}$.

$$F_s = S * F_{s,max} \tag{2.1.2i}$$

Mobility is possible if the shear force developed by the track F_s exceeds the sum of the motion resistances. In other words, motion will occur if the value for the drawbar pull in *Equation 2.1.2a* is positive. It is important to note that the tractive force in *Equation 2.1.2h* is only applicable to a tracked vehicle. The maximum tractive force that other drive mechanisms can develop (custom paddlewheels, screws, etc.) has not been extensively studied. Further research must be conducted to estimate the tractive force developed by these alternative drive methods. The condition for motion in a general sense is therefore the relation shown in *Equation 2.1.2j*, where F_p is the tractive force developed by a vehicle using any drive method, and ΣR_f is the sum of all motion resistance forces.

$$F_p > \Sigma R_f \tag{2.2.2j}$$

2.1.2.4. Torque Requirement

Once all the resistances are found and drawbar pull calculated, the minimum torque a drive mechanism must provide to achieve said drawbar pull can be found. The minimum torque required by a vehicle's driveline must generate a driving force at the interface of the terrain more than the tractive force in *Equation 2.2.2j*. The tractive force is the most critical parameter for motion in snow, but the driveline must be able to generate that force at the terrain interface. In a rotating drive wheel or sprocket, the force developed at the terrain interface is equal to the torque generated by the drive wheel divided by the torque lever arm. The lever arm *R* can be thought of as the radius of the wheel for wheeled vehicles or the radius of the drive sprocket for tracks. When designing a drivetrain, it is recommended to include a safety factor to increase the available torque of the system to account for resistance variability and other losses.

2.1.3 Snow Buildup

Another important design consideration for traveling on snow is the prevention of snow from building up inside critical drive components like pulleys, gears, and treads, shown below:

Figure 2.2.3.1 - Buildup of snow in key drive components [9]

Cohesive, wet snow is more likely to stick to internal driving components and clog mechanisms. Lever, Shoop, and Bernhard designed a different snow robot that included large cavities in the housing that were harder to fill with snow and easy to clean by hand. Small, hard to reach cavities are easy to fill with snow during use and can clog main drive mechanisms.

2.2 Modeling Motor Power, Torque Requirement and Battery Life Requirement

The following models were created to calculate the minimum required power and traction needed for a propelled snowboard. For torque, since it is dependent on a design dependent lever arm, the main component to focus on is the traction or tractive force needed to climb a hill (F_P). *Figure 2.2.1* models the forces the device would experience when traversing a hill.

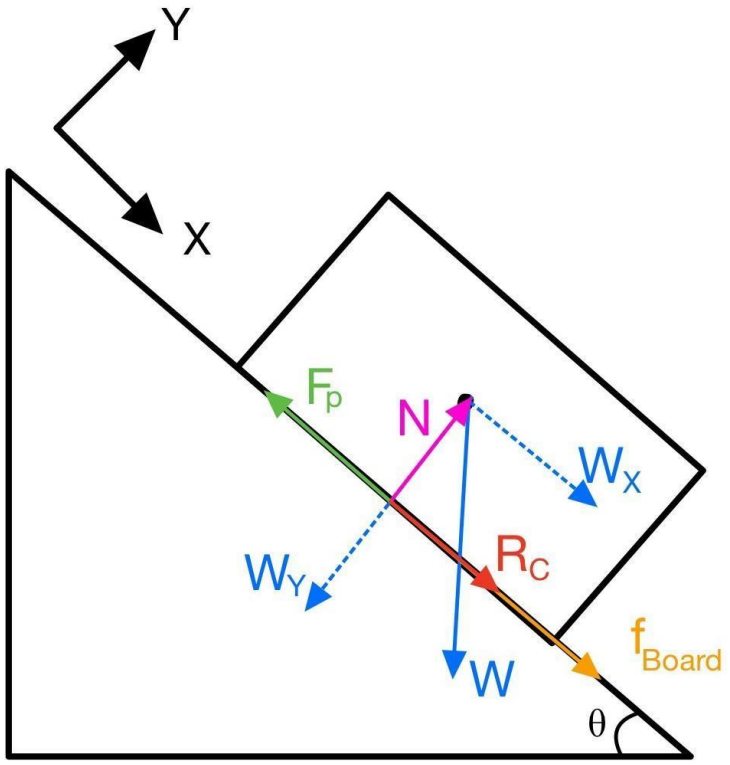

Figure 2.2.1 - Motor Torque Free Body Diagram for Propulsion Mechanism on a Hill

In *Figure 2.2.1*, W represents total device and rider weights, N is the normal force, R_C is the compaction resistance, and f_{Board} is the friction between the snowboard and snow. W is split into its components along the x and y axes of the coordinate frame which are defined below.

$$W_X = Wsin(\theta) \tag{2.2a}$$

$$W_Y = Wcos(\theta) \tag{2.2b}$$

R_C is defined using *Equation 2.1.2c* or *Equation 2.1.2d* depending on the drive mechanism. θ is the hill incline angle in radians which can be found from the hill grade using *Equation 2.2c*: $\theta = arctan(\frac{HG}{100})$. From the diagram the following equations can be defined.

$$\Sigma F_X = 0 = -F_P + R_C + f_{Board} + W_X \tag{2.2d}$$

$$\Sigma F_Y = 0 = N - W_Y \quad (2.2e)$$

Solving the above equations for F_P, the resulting equation (*Equation 2.2f*) can be used to determine the minimum force that must be exceeded to propel the snowboard forward.

$$F_P = R_C + \mu_{Board} W cos(\theta) + W sin(\theta) \quad (2.2f)$$

The minimum power and torque to overcome resistances can be found by multiplying F_P by the average expected velocity of the propelled snowboard and the radius of the drive wheel respectively. To note, for power calculations, the estimated minimum power is based on constant flat ground travel. Therefore,θ would be 0 and *Equation 2.2g* would be used to solve for F_P.

$$F_P = R_C + \mu_{Board} W \quad (2.2g)$$

The above models for calculating power and torque serve as the minimums needed for the device to operate due to working assumptions. The main assumption is that bulldozing resistance is negligible because the weight of the bulldozed snow is insignificant compared to the weight of the device. To solve the models for our device, the following parameters need to be defined as part of the requirements to determine the required minimum motor power and battery capacity. These are shown in *Figure 2.2.2*.

Parameter	Description	Units
W	Combined weight of the board and rider	N
v	Top speed of the device	km/hr
θ	Hill incline angle	radians
t	Time the device will run for on a single charge	hours

Figure 2.2.2 - Required Parameters to Calculate Minimum Motor Torque and Battery Capacity

2.3 Snowboarding Turning

Instead of incorporating a differential steering mechanism into our design, we plan to incorporate lean steering, which is how riders control modern snowboards. To understand how riders turn, we first will look at turning the Snurfer, the grandfather of the modern-day snowboard, and then discuss the two ways a modern snowboard turns, skidding and carving.

The Snurfer consisted of two skis bolted together, a nose-mounted steering rope, and no bindings. The rider would pull rope connected to the tip of the board which would decrease ground contact on the nose. This would create a pivot point behind the back foot, about which the rider can turn. According to the patent, this turning required more skill and athletic capability

than skiing [13]. As the invention was refined, bindings were introduced and the rope was removed, which made it easier to turn.

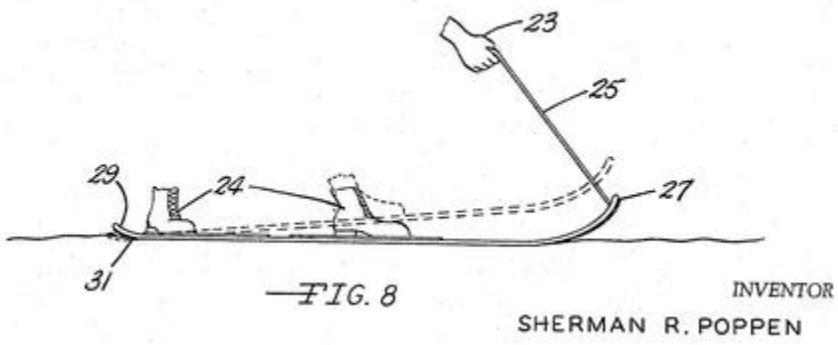

Figure 2.3.1 - Snurfer Patent [13]

To maintain the feel of snowboarding, lean steering is integral to our design. In modern snowboarding there are two main ways to turn when riding a snowboard, skidding and carving. Skidding greatly reduces the speed through a turn and the board is perpendicular to the arc of the turn, the velocity of the rider is perpendicular to the board. This creates a plowing motion as snow is pushed by the board, creating friction because the edge of the board is lifted in this maneuver allowing snow to build up underneath [14].

Carving, the other snowboard turning maneuver, tends to have a larger radius than skidding. In a carve, the board is in line with the side edge curvature and parallel to the velocity of the device along the arc. Carving is a more gradual turn compared to skidding, and the general size of the curve is based upon the side cuts in a snowboard. Modern snowboards are designed with a reverse camber, or an arch built between the bindings, which allows the rider to carve properly if the board is at an angle with the snow [14]. The angle between the board and the snow, the rider shifting their weight into the turn, and the board flexibility allows riders to form a tighter curve than the curve of the side cuts on the board [15]. The sharpness of the curve is defined by the arc the turning edge makes with the snow and as a rider shifts their weight into the turn it deepens this arc leading to a sharper turn.

2.4 Relevant Devices

In addition to modern snowboards, other recreational devices are available which we took inspiration from. The original inspiration for our project is an electric skateboard as that is what the team is most familiar with. Another source of inspiration is the snowmobile. In addition, while the field of powered snowboards is not fully developed, there are still many prototype designs and even a few boards on the market.

2.4.1 Electric Skateboards

Electric skateboards are currently the dominant propelled board product currently on the market; several variations are commercially available. They serve as a great analog for the performance specifications that would make our device entertaining. In addition, they provide some statistics that hint at the type of people in the potential market for a propelled snowboard. Comparing various popular electric skateboards, particularly off-road models, the following statistics were generated for what could provide an entertaining ride. These specs also provide estimates for expected performance of our device from the potential market. A list of the electric skateboards used for this are in *Appendix 6.B*.

Performance Specification:	**Range:**	**Average:**	**Units:**
Top Speed	35.4 - 59.6	45.6	km/hr
Range	17.7 - 96.6	46.0	km
Max Hill Grade	25 - 46	33.6	%
Battery Capacity	345.6 - 2152	775.1	Wh
Max Rider Mass	90 - 247.95	133.9	kg
Board Mass	9.4 - 108	10.07	kg

Figure 2.4.1.1 - Ranges and Average Specifications of Commercially Available Electric Skateboards

The two most directly applicable specifications are rider weight limit and board mass. When it comes to the rest of the specifications, they are less applicable but are useful for reach-goals to increase the device's marketability. For example, compared to asphalt, snow requires more energy to traverse over, thus our device would require more torque and power to meet electric skateboard standards. To help handle soft terrain like snow, off road electric skateboard companies employ modifications to improve performance.

A common technique for enabling electric skateboards to traverse dirt and soft terrain is enlarging the wheels to increase ground clearance and adding large tires for flotation. For a smoother ride, some electric skateboards include spring suspension to the trucks. However, electric skateboards are not designed for riding in snow and rely on static friction to propel themselves, which is prone to slipping in soft terrain. As a result, the specifications above, particularly battery capacity and top speed, serve best as reach-goals rather than targets.

With regards to user input, besides lean steering, electric skateboards commonly utilize remote throttles for the rider to control the speed. The major advantage of remote control is that there is no cable, thus no risk of snagging on nearby objects or the rider themselves. Also, there

is no concern for cable degradation from pulling and flexing and no worry of breaking the cable when the rider falls off the board. However, in the case of snowboarding, riders are strapped to the board reducing the potential issue of breaking the control cable. Therefore, both wired and wireless throttle control were considered for this project.

2.4.2 Snowmobiles and other Single Person Snow Vehicles

A popular powered snow traversing vehicle is the snowmobile. In addition to recreational uses, snowmobiles are used for transportation, hunting, and trapping. In remote locations, these devices are the main transportation method when roads are closed due to snowfall. Generally, a snowmobile is a sled with front skis and tracks in the back. A snowmobile is turned using a handlebar system like an ATV or a bicycle. Snowmobiles tend to be gasoline powered, which can lead to pollution and noise problems [16].

A newer-to-market design is an electric snowmobile produced by Taiga, the Nomad. Electric snowmobiles can apply instant torque to the system with zero latency. The battery on the Nomad can reach 80 percent charge in 20 minutes and has an estimated range of 134 km under ideal conditions. A disadvantage many electric systems encounter at lower temperatures is that colder temperatures can negatively impact battery life. The Nomad reduces this problem by including a thermal management system, which can cool or heat the battery pack, which leads to a maximum loss of five percent in extreme cold. This thermal system takes about six minutes to preheat before the snowmobile is ready to ride unless the system is plugged in before use to keep the battery at temperature [17].

2.4.3 Powered Snowboards

There are a few powered snowboards on the market or in production, including Mattracks Power Board, Power Traverse and the Skizee. The Mattracks Power Board, found in Figure 2.4.3.1, uses a track system like a handle for steering but can carve like a snowboard. This board has a six and a half horsepower gasoline engine which allows the engine to reach maximum speeds of 18 miles per hour and run for up to two hours. The chassis is mainly aluminum and features a tread system for mobility of the device [18].

Figure 2.4.3.1 - Mattracks Power Board [19]

The Power Traverse, found in Figure 2.4.3.2, is an electric powered board with a paddle wheel at the back to propel the board. It is currently still in the process of prototyping. The design puts the batteries on the user's back, inside of a custom-built insulated backpack. It uses a hub motor to move the vehicle, which is custom built to adapt the blades of the paddle wheel which are attached with magnets. The device has ten 20Ah battery packs with an estimated run time of 300 minutes [20]. The information for this device was obtained from an Instagram account run by the builder of the device so information was hard to find. The creator is planning to take the device to market, so the owner is intentionally making the design choices not as clear.

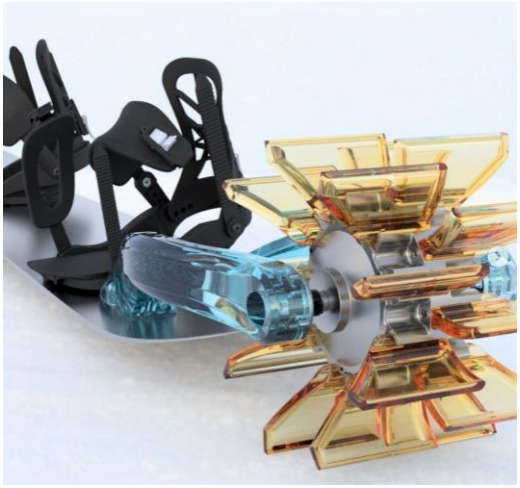

Figure 2.4.3.2 - Power Traverse [20]

The Skizee is not quite a powered snowboard, but it is a way to drive a snowboard or skis over flat ground. The system was designed for a skier, but the system can function with a snowboard. It has a 4-stroke engine with a one-gallon gas tank with a twelve-volt six-amp hour battery for starting the system and accessories like lights. The device pushes the skier, who holds

onto two handles, with a tread system. The Skizee emulates a snowmobile with the skier's skis as the front skis and a powered motor tread in the back. The two handles fold into the system during storage to reduce the size of the system, however the system still weighs 130 pounds. The skier and Skizee can travel up to 40 km per hour, but the standard operating speed is 25 km/hour. With the one-gallon tank, the Skizee can travel about 50 kilometers, or two hours at 25 km/hour. The price point for this system is about CA$5000 [21].

Figure 2.4.3.3 - Skizee Woodsrunner[21]

In addition to consumer electric snowboards, there are many prototypes and hobby projects accessible online. Hacksmith Industries has created two different prototypes, a fan-powered device, and a jet engine design. The fan powered device is lithium-ion battery powered and features two electric ducted fans stacked on the back of the device for propulsion. It did not have electronic steering, and instead relies on the ability of the user to turn like a snowboarder, but was unsuccessful at higher speeds, so the team was unable to reach top speed for the device. The battery only has a 5-minute run time, so the current design is not feasible as it requires too much energy for desirable run times [22]. The Turbo device was a "one day" build, so it is safe to assume not as much design work was put into the project. In sum, the team mounted an old jet engine to an existing snowboard. The jet engine is Kingtech K320g which produces 32 kilograms of thrust and is powered by diesel. The speed control on this device was hardwired to the device. This design had problems with steering, as the center of pressure was in front of the center of mass which led to spin outs. To ride it properly the user had to shift most of their weight to their front foot, which was said to be exhausting [23].

Figure 2.4.3.4 - The Hacksmith's Fan Snowboard [22]

Figure 2.4.3.5 - The Hacksmith's Jet Engine Snowboard[23]

Another prototype design is the Propul~Surf, a screw-propelled vehicle. It uses hub motors to drive the system alongside LiPo batteries. The prototype is slow as it can only reach speeds of 7.5 km/hr. The final design for the device has all components inside the screws, such as battery and AC drives. The team designed the device with a low screw thread to increase the torque that could be transmitted to the device. The device was controlled with a wired remote. The prototype was featured on the United Kingdom's *Gadget Man,* with poor results as the device was unable to push the board with the user, but the team does have footage from their own tests of the device working, but as previously stated it moved slowly [24].

Figure 2.4.3.6 - Propel~Surf[24]

We came across a few more prototype designs such as the SnoDeck from the University of Waterloo, The Augerboard from Mototcamokat and the Electric snowboard from Homemade Mehanol. All these prototypes had interesting design choices, but we were unable to find in depth information. The SnoDeck used two sets of tank treads on a skateboard base instead of wheels and can be found in Figure 2.4.3.7 [25]. The energy system appeared to be contained inside of the treads and we assume the system is battery powered. The SnoDeck is an older device, and the only video available dates to 2007. The Augerboard, as the name suggests, has two long screw mechanisms on the sides of a sled base, which the rider either sits or stands on [26]. The video of this device shows it moving faster than the Propul~Surf. The Electric snowboard from Homemade Mehanol has two prototypes which work similarly, one with a giant tire and one with a smaller tire with raised fins for gripping the snow [27]. Both prototypes use a mechanical tiller like a sailboat to turn, with speed controls on the tiller. The videos of these devices show them working well, but it is unclear how they are powered again, we assume using the device is using electricity due to the name.

Figure 2.4.3.7 - SnoDeck [25]

Figure 2.4.3.8 - Augerboard [26]

Figure 2.4.3.9 - ElectroBoard from Mehanol [27]

2.5 Background on Critical Components

The final prototype of the electric snowboard includes a battery, handheld remote, motor and motor controller. Critical components will be selected based on their expected performance in a cold, snowy environment.

2.5.1 Electric Batteries

Most personal electric vehicles run on lithium-ion batteries as these devices cannot be tethered to an electrical power outlet. In addition, lithium-ion batteries are more widely available and better suited to this application than nickel or lead acid batteries. Electrons within a battery flow from a negatively charged material (anode) to a positively charged material (cathode). The ions within the anode lose electrons as they move through the electrolyte, towards the cathode. The motion of electrons from the anode, through the circuit to the cathode, creates electric current. Once all the metal components of the battery have been oxidized, the battery is depleted and must either be recharged or thrown out. Because a battery's function is based on a chemical reaction, battery performance is dependent on temperature. Cold temperatures hinder battery performance as it relies on an oxidation reduction reaction to induce an electrical current within a circuit. If the battery is to be operated below 32° Fahrenheit or 0° Celsius, the chemical reaction that triggers the current flow will slow down and eventually stop.

Winter weather is notorious for damaging car and cell phone batteries. The cold temperatures reduce the rate at which oxidation occurs by increasing the internal resistance within the battery and reducing the ionic conduction. Battery capacity is reduced by as much as 50% in temperatures below freezing [28]. Battery life is cut in half every 15° F over 77° F. Cold

cranking is useful to determine how batteries will perform in low temperatures. Cold cranking is the discharge current from a fully charged battery operating at 0° F; the cold cranking current is lower than the current at room temperature. The battery we select for our system must deliver sufficient current to the motors to overcome stall current over the operating temperature ranges.

2.5.2 Electric Motors

The purpose of an electric motor is to convert electricity to mechanical power, which is produced in the form of a rotating shaft. Although AC power motors are available, we favored DC motors for their wide availability, compatibility with electric batteries, and quick response to current variation. Two types of DC motors are available today; brushed (BDC) and brushless DC (BLDC) motors.

The brushed (BDC) motor is composed of two basic components: an armature, which rotates when electrical current is applied and a stator, the stationary components of the motor. Permanent magnets with opposite polarities are fixed inside the stator. Attached to the armature is a rotor, which consists of a set of arms wrapped in electrical coils. When electrical current is passed through these coils, it generates an electromagnetic field. Turning on and off separate branches of the coil in sequence creates a rotating magnetic field which spins the armature. In BDC motors, an electrically conductive component called the commutator is attached to the motor shaft and allows a full circuit to be established. The commutator transfers and splits current from the power source evenly between the coils present in the motor. When current is fed through the coils of wire, a magnetic field is generated between the electromagnets and the permanent magnets in the housing. The permanent magnets are mounted to the stator, and the electromagnets are mounted to the spinning armature.

Within brushless DC (BLDC) motors, this orientation is reversed; one or more permanent magnets are installed in the rotor, and the electromagnets are set on the stator. BLDC motors are divided into internal and external rotor configurations. External rotor BLDC motors are fixed in the center, and the outer housing spins around the motor shaft. These motors can develop a higher torque than comparably sized internal rotor motors. In electric skateboards, these are commonly referred to as “hub motors” and are often mounted inside of a wheel without any gearing. The Power Traverse board features an external-rotor BLDC motor to spin its paddlewheel. Internal rotor BLDC motors are also used in electric skateboards with gearing and/or drive belts to spin the wheels. In BLDC motors, a motor controller is needed to charge the correct coil to maintain magnetic potential energy within the motor and keep the rotor spinning. Since the magnetic polarity is controlled electronically, BLDC motors are said to be “electronically commutated”. This prevents the need for a physical commutator mounted to the rotor. Brushless DC motors were favored for use in this project for their long life, high efficiency, low maintenance and high-power density.

2.5.2.1 Motor operation concerns

A major concern with electric motors under continuous use is overheating. NEMA, the National Electrical Manufacturers Association, determined that for most motors the maximum rated operating temperature is 180 ℃ or less [30]. In addition, a motor operating every 10 ℃ above its rated operating temperature will reduce its life in half. It is important, therefore, to select a motor whose maximum rated temperature class best fits its intended operating environment. On the other hand, there is no minimum operating temperature rating on electric motors because they heat up during use. In addition, snow can clog motor vents causing the motor to heat up faster. This can force the motor into service temperatures above its rated operating temperature [31]. Electric motor safety comes mainly from properly selecting a motor for its application and operating environment. Physical danger can arise in the form of pinch points when rotating components are left exposed to the end user; for this reason, these components are often covered.

2.5.3 Electronic Speed Controllers

Electronic Speed Controllers (ESCs) are circuits which control the voltage of an electric motor. Some ESCs feature settings for different skill levels, safety features, and even dynamic braking. As a result, the ESC has become the main computer for many electric personal vehicles including skateboards, bikes, and scooters. In addition, especially with electric skateboards and drones, the ESC includes a wireless transceiver module for communicating with a remote control. Due to the similarities between our device's electrical needs and that of an electric skateboard, many ESCs that are designed for electric skateboards will work for this project.

There are two main types of ESCs for electric skateboards, proprietary and VESC. Proprietary ESCs are complete black boxes that are only compatible with the manufacturer's remotes and lack customization. LingYi and Hobbywing are two such proprietary brands. VESC, on the other hand, is an open-source ESC that is compatible with a software tool, VESC tool, enabling users to fully customize the behavior of a motor. The customization includes throttle curves, safety features, and the ability to interface with custom components such as Arduinos [32] [33]. In addition, there is a complementary Android app for monitoring speed, battery power, and connection status. VESCs, and ESCs in general, are also only compatible with certain motors based on the current rating and type of the motor.

To prevent destroying the ESC, it needs to be able to handle the required current draws of the chosen motor, continuous and burst current. ESCs can often handle bursts of current higher than the continuous rating but only for a few seconds [34][35]. The burst rating is dependent on the quality of the ESC parts and therefore varies between ESCs. In some cases, the burst current is even double the continuous current. VESCs and other electric skateboard brands also list a continuous current rating which is the current draw of the motor. Typically, the continuous rating is used as the base requirement for the ESC current capability with a margin of error of 20% to account for inefficiencies from the ESC and the motor. The same safety factor is used for the

current draw of the battery by the ESC. In addition, the ESC has a safe voltage range to ensure proper operation which the motor must operate within. Lastly, ESCs are only able to control either a brushed or brushless motor due to the inherent difference in motor behavior. In the electric skateboard market, there are almost no brushed motors available. Furthermore, VESCs only work with brushless motors because the software is based on a tool designed for brushless motors, the BLDC tool [36].

3.0 Design Requirements

The device was designed during this project to meet the specifications in *Figures 3.0.1* and *3.0.2*. These constraints are described in more detail below, separated into two categories: board requirements and environmental requirements.

Category	Name.	Description	Value	Units
Board Requirements	Max Size	Length	180	cm
		Width	60	cm
		Height:	46	cm
	Maximum Board Mass	**Target**:	**25**	kg
		Nice to have:	18	kg
		Reach:	13	kg
	Maximum Level Velocity	**Target**:	**4.5**	m/s
		Nice to have:	6.7	m/s
		Reach:	9.8	m/s
	Battery life*	**Target**:	**1**	hrs
		Nice to have:	2	hrs
		Reach:	3	hrs
		*Measured assuming constant level ground and three fourths the max velocity		
	Rider Mass Limit	**Target**:	**63.5**	kg
		Nice to have:	104	kg
		Reach:	113	kg
	Waterproofing	IP64		
	Noise	88 dBA		

Figure 3.0.1- Board Requirements

Category	Name	Description		
Board Requirements (Cont.)	Safety	No pinch point locations		
		No exposed high voltage wiring or connectors		
		No accessible sharp edges		
		Does not have risk of creating a projectile		
		Rider will not be able to operate the board when not properly attached or on the board		
	Ergonomics	The control interface must be able to be operated with winter gloves		
	Maintenance	The device must be able to be cleaned and maintained without the need for special tools.		
		Any snow that builds up within the drive mechanism must be able to be cleared easily and continue operating normally.		
Environment Requirements	Temperature	**Target**:	**-6**	℃
		Nice to have:	-12	℃
		Reach:	-18	℃
	Hill grade	Minimum Climbable Incline	10%	
	Snow Density	Able to traverse powder and groomed snow	150-500	kg/m^3

Figure 3.0.2 - Continued Board Requirements and Environmental Requirements of the device

3.1 Further Explanation of Board Requirements

3.1.1 Board Requirements

Board Size

The board must be no more than 180 x 60 x 46 cm (~6 x 2 x 1.5 ft) measured in board length by width by height. This represents a volume that can be reasonably carried by the rider without being uncomfortable to hold, while still giving the team ample room for ground interface and bindings.

Board Mass
The target board mass is equivalent to the recommended maximum mass an object should be held over 8 hours [42]. The reach is based on the average electric skateboard weight. For, the nice-to-have goal is half of the reach.

Max Rider Mass
The target rider mass is based on the average mass of members of our team. The reach goal is equivalent to the standard rider mass limit of an electric skateboard.

Board Speed
Board speeds are based on velocities of similar products on the market. The target speed is comparable to lower-grade electric skateboards offered for less than $200. The nice-to-have and reach goals are similar to speeds of higher-grade electric skateboards typically available.

Speed Control
The board must be able to be controlled via a handheld remote to control speed. The handheld controller shall be able to be operated while wearing winter gloves and shall achieve the same waterproofing rating as the board (see "Waterproofing Requirement").

Battery Life
The target requirement represents a common battery life of typical electric skateboards on the market today. Most electric skateboards last about one hour on a charge; the nice-to-have and reach goals represent challenges that would boost the performance of the board if they were achieved.

Waterproofing Requirement
The board shall be constructed to meet the IP64 waterproofing standard to protect inner electronics. IP64 is defined as "protected from dust ingress and protected from water spray from any direction"[49]. IP64 was selected to represent the environmental conditions of riding through snow. While "wet snow" conditions are common in the winter, it is unlikely the device must be fully liquid submersible. Any snow that melts to liquid on the device is considered by the team to be comparable to "water spray" as defined in the IP index.

Max Decibel Requirement
Noise generated by the board while running shall not exceed 88 dBA. This represents a safe volume for 4 hours or less of continuous sound according to the American Speech-Language Foundation [43].

Temperature

Temperatures represent a minimum intended operating temperature for the device. The target temperature of -6 C represents the lower bound of the preferred alpine skiing temperature range [44].

3.1.2 Environmental Requirements

Intended Use Terrain

The board is intended primarily for use in snow, having densities from 150-500 kg/m^3. This comprises the following snow types:

- Fresh Snow or "Powder": 150-200 kg/m^3
- Settled Snow: density between 200-300 kg/m^3
- Compacted or Groomed Snow: 300-500 kg/m^3

This represents the snow types that are typically seen on the ground, ranging from back-country trails to groomed resort conditions. These are expected to be the most common types of snow a rider may encounter and represent the terrain the device should perform the best on.

Traversable Incline

Snowy terrain often consists of hills and valleys which a rider will seek to traverse. The device must be able to traverse a 10% incline. This represents a moderately steep incline for most roadways, and an upper limit gradient for most hiking trails [45]

3.2 Derived Requirements

3.2.1 Surface Area to Maintain Flotation

Using the contact pressure found in Section 2.2.1 of 3,330 Pa and an intended maximum system weight of 883 N, the resulting required supporting area is found to be 0.33 m^2 using *Equations 3.2.1a* and *3.2.1b* below.

$$\frac{883\ N}{a\ m^2} = \frac{3{,}330\ N}{1\ m^2} \tag{3.2.1a}$$

$$a = \frac{883\ N}{3{,}330\ N/m^2} = 0.27\ m^2 \tag{3.2.1b}$$

From the board size requirement in Section 3.0, the maximum board area the device can have is 1.08 m^2. Thus, the max size and minimum flotation pressure dictate that the device must have a surface area between 0.27 m^2 and 1.08 m^2. As a snowboard deck has a surface area of about 0.27 m^2, the minimum surface area requirement can be met if the electric snowboard has a comparable ground contact area.

4.0 Methodology

The propelled snowboard consists of five major systems: propulsion, chassis, suspension, power, and control. The propulsion system includes the ground interface and the motor that supplies the propulsion force to move the device. The chassis supports the ground interface. The suspension applies an adjustable downward force on the chassis to ensure the device develops sufficient traction for different snow densities. The power system is the battery that powers the control systems. The control system consists of the rider input and internal control mechanisms to ensure the device performs in the best conditions. The final system design can be shown in *Figure 4.0.1* below.

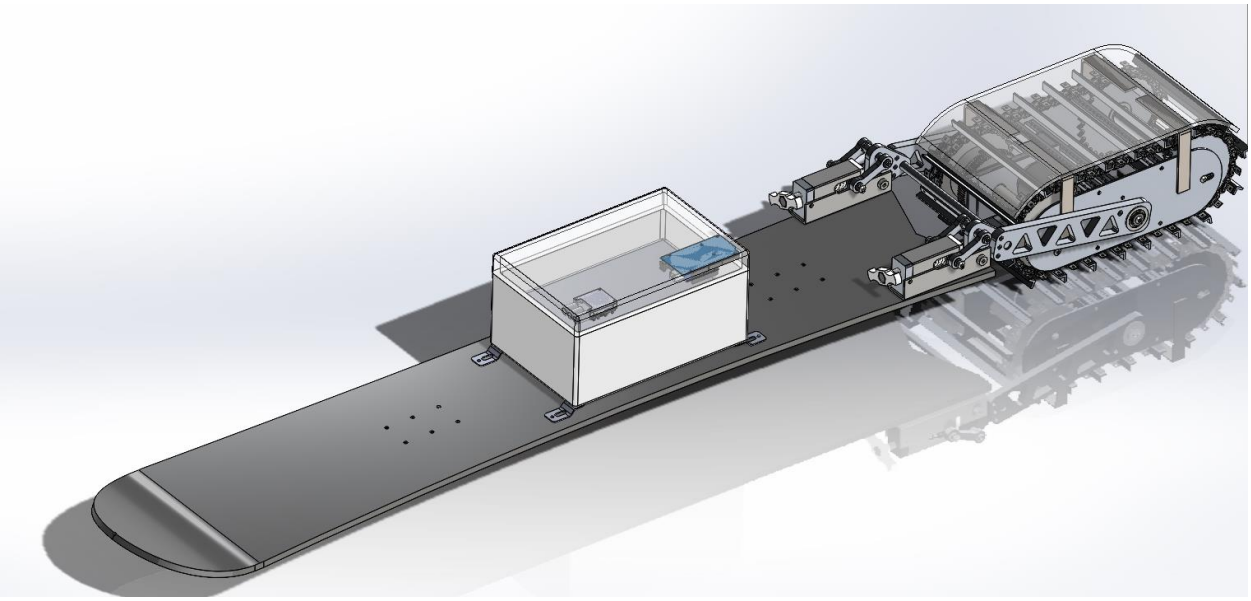

Figure 4.0.1 - Final System Design of the Electric Snowboard.

4.1 Propulsion

4.1.1 Brainstorming and initial designs

During initial research, the team brainstormed a list of 12 different ground interfaces. A ground interface is the method for developing traction and the system that contacts the snow. The team has decided to further iterate on four main designs based on market research and discussions on each design’s feasibility. The team refined these designs through a circle sketching process where each of the members could add features and suggest modifications. These circle sketches can be found in *Appendix 6.B.*

The first design the team developed was a tread system, which is like the Mattracks PowerBoard. In the team's design, the treads were placed between the legs of the rider and the

sides of the board could still be used for carving (Figure 4.1.1.1). The natural symmetry of this device allows for the rider to lead with either foot, assuming the treads could be driven backwards. The team foresaw that the tracks add significant weight, and there may not be sufficient room between the bindings to place a tread system while maintaining adequate bending strength to be able to turn.

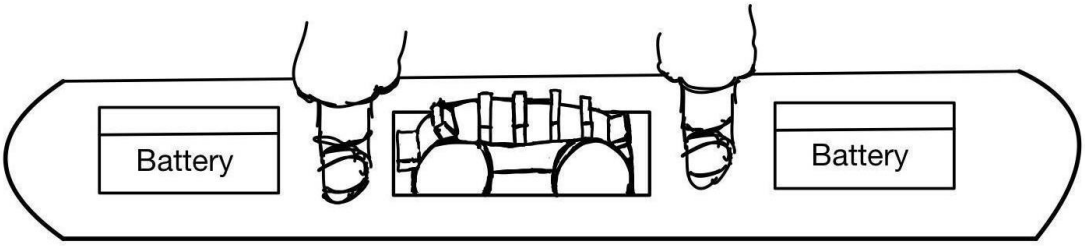

Figure 4.1.1.1 - Sketch of Central Track Ground Interface

The second design was a screw drive, or auger drive, like the Propul~Surf, but instead of the screws at the end of the board, they are between the rider's feet (Figure 4.1.1.2). Again, the center driving system should improve the stability and turning mobility of the board and lead to a smoother ride. The large driving screws would add weight, and a prior MQP expressed that it was hard to guarantee symmetrical speeds between the motors, which leads to directional drift. Lean steering on this system could be difficult due to screws extending below the board, counteracting the lean of the rider. Additionally, the devices we found that used auger drive were very slow because a lot of energy was wasted pushing perpendicular to the desired direction of motion.

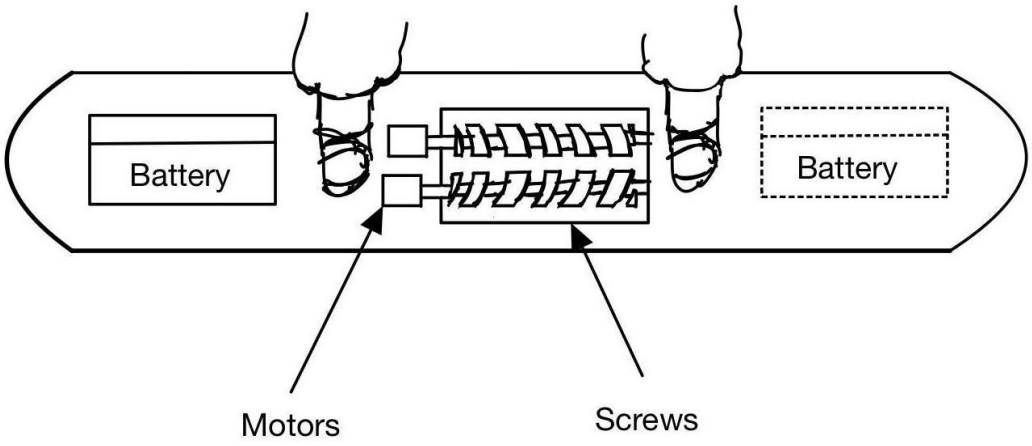

Figure 4.1.1.2 - Sketch of Auger Drive Ground Interface

The third design was based on a steam or paddle boat with a large back wheel for pushing the snow, similar to the Power Traverse board (*Figure 4.1.1.3)*. The wheel could shift the center of weight to the back of the board, allowing the front to push above the snow while the paddle

wheel is able to push the most snow. This sinking in the back would cause the system to push more snow than if the weight was distributed equally [5]. A wheel has only one location to push the snow fully forward which is at the bottom of a wheel, so the more the board compacts this snow the easier it will be to push. But this shifting of the weight could make it harder to turn as the location of the applied turning force would be in front of the center of mass and propulsion system.

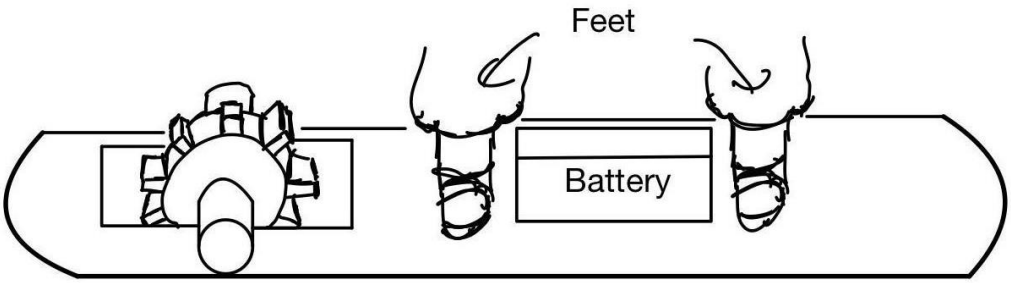

Figure 4.1.1.3 - Sketch of Single Paddle Wheel Ground Interface

The last design the team is considering is a double roller design with a roller in the front and the back (*Figure 4.1.1.4*). This design is the one most like the original catalyst for our project, an off-road electric skateboard. This design features either paddle wheels like the third design or wheels more like foam rollers for exercise, but sturdier. This design could lead to most of the load being split along 2 axes instead of along the full plane of the board.

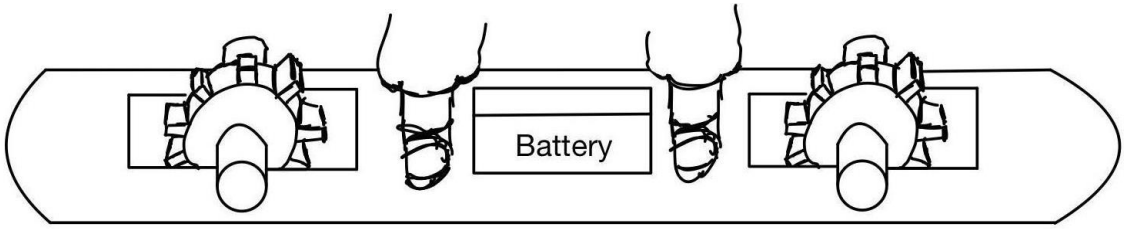

Figure 4.1.1.4 - Sketch of Dual Paddle Wheel Ground Interface

4.1.2 Mini-Prototype Testing

Through research the team was able to narrow down the potential propulsion methods to two options: treads or paddlewheels. However, our research was not sufficient to determine the better solution, so a smaller scale test was devised. Treads and paddlewheels were selected for testing because they showed the most success in existing products and possessed the highest interface-to-ground force transfer efficiency. We defined force transfer efficiency as the amount of tractive force developed by the propulsion methods (in Newtons) per amps consumed. Treads

possess the highest force transfer efficiency because their grousers are perpendicular to the snow for the largest percentage of the contact patch, so their force transfer efficiency is high. The force transfer capability is next highest in a paddlewheel; however, their grousers are perpendicular to the snow (and thus develop their maximum amount of pushing force) at only one point in the wheels motion. Despite its novelty, screw drive was not tested because a significant portion of the force is wasted pushing snow in a direction perpendicular to the direction of motion. Dual paddle wheels were also not tested because the method was too complex to build and is not significantly different from the single paddlewheel.

The goal of our prototyping was to see if each system could successfully develop enough tractive force to move forward and to gather hands-on experience with both systems. The dependent variable in our testing was the tractive effort standardized by the contact patch. The contact patch was calculated using the largest area the device had when in contact with the testing medium. The tractive effort was standardized to eliminate the differences in contact patch among the different systems. The drawbar pull, as defined in *Equation 2.1.2a*, was measured by a strain gauge sensor.

The testing rig was designed to accommodate scaled down designs of both a track system and a paddle wheel system. A 41 cm plastic hand board was used as a stand-in for the snowboard, the tail was removed on the board and the testing rig, which can be found in Appendix 7.F, was attached with hot glue. During testing the board bowed which led to a quick fix of a wooden brace which added rigidity to the board. The team used moist sand as a mock compressed snow. This material was selected for its availability and similar properties.

The track system was designed using VEX robotic components, which allowed for the length of the grousers to be changed swiftly. Three different lengths of grousers were considered: 12.7 mm, 22.9 mm and 33 mm. The paddle wheel systems were 3-D printed polylactide (PLA) parts which were designed to interface with the Vex components already present in the testing rig. The drive chain was moved upward to allow for a similar number of paddles interfacing with the mock snow. Three different wheels were designed, two sizes of flat wheels and a scooping wheel, these can be found in Appendix 7.F.

The electronics of the prototype were a voltage supply, an Arduino, an on/off switch, and a DC motor. The motor was a 12V Pololu 50:1 gearmotor with an encoder. The Arduino code was designed to allow for a gradual increase of current to the system until the motor was able to start pulling the prototype forward.

4.1.3 Results of Prototyping

After reflecting on the small-scale prototype results and methodology, the team decided a track system would be the best option. The team observed the tread system was more stable and less likely to tip than the paddle wheel. The paddle wheel system was less stable because it contacted the testing medium with less grousers than the tracked system. The scooping paddle

wheel did not demonstrate any significant improvement in stability over the straight grouser paddle wheel.

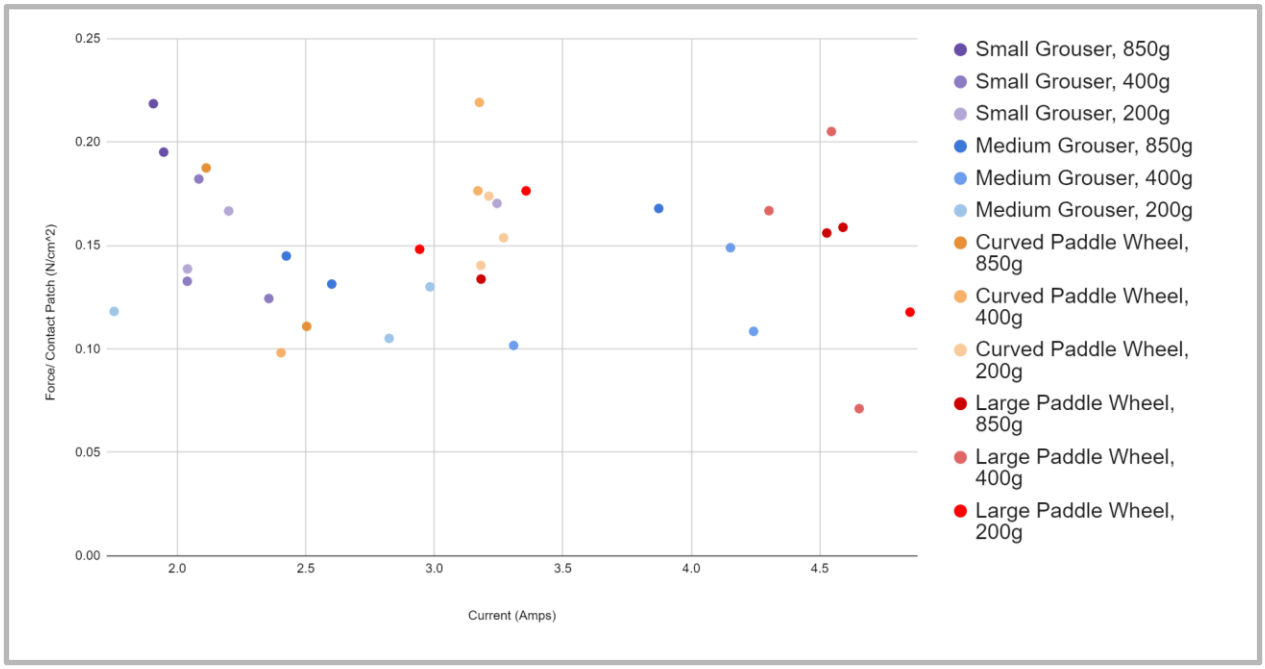

Figure 4.1.3.1 - Max Current vs Max Force per Contact Patch Results from Mini Prototype Tests

Figure 4.1.3.1 plots the peak force developed divided by the contract patch calculated for each system versus the current. Both the current and drawbar pull force were averaged over 10 timesteps to eliminate large noise spikes. The small grousers, indicated by purple dots in Figure 4.1.3.1, required the least amount of current and exerted the some of the highest drawbar pull readings. Pulling lower amps is better for our design as it would allow our full-scale prototype to run at a lower current. It also signifies that the motor torque to move the system is lower. The small track system had higher drawbar pull values than the medium grocers indicating it developed more force. Treads required less current to produce the same amount of force per contact patch than paddle wheels. This made them more efficient and generated traction.

4.1.4 Determining Minimum and Maximum Tractive Effort

4.1.4.1 Compaction Resistance

To calculate the total tractive force for propulsion, the estimated compaction resistance must be calculated. To estimate compaction resistance, values for terrain constants are borrowed

from Wong [5] for snow in Colorado, USA. These terrain coefficients are defined in *Figure 4.1.4.1.1* below, along with the other variables needed for *Equation 2.1.2c*.

Variable	Value	Units
n	1.6	unitless
k_c	4.37	kN/m^{n+1}
k_φ	196.72	kN/m^{n+2}
b	0.216	m
l	.356	m

Figure 4.1.4.1.1 - Terrain values and track dimensions for snow in the United States

Other variables must be defined or assumed to specify the tread geometry used in the compaction resistance estimate. In these assumptions, the track width b of 0.216 m and board length of .356 m are used to approximate the final ground interface geometry, and an overall weight of 883 N is used. These width and length measurements represent the approximate width and length of a track that is the same size as a snowboard tail. A compaction resistance of $R_c = 6.5N$ was then found using *Equation 2.1.2c* for tracks.

4.1.4.2 Calculation of F_p

The total tractive effort that must be developed by a snow vehicle to achieve motion must exceed the sum of all motion resistances, as derived in *Equation 2.2f*. The sum of all motion resistances is equal to F_p. Motion occurs when the developed tractive force F_s exceeds F_p. The total motion resistance was calculated using *Equation 2.2f* which includes frictional resistance between the board and the snow and the compaction resistance. These values are shown below in *Figure 4.1.4.2.1*. F_p calculated as the sum of the frictional resistance and the compaction resistance which is 95 N.

Total system weight (W)	883 N
Friction coefficient between board and snow (μ_{Board})[10]	0.1
Incline angle (θ)	0.1 radians
Compaction Resistance (Tracks)	6.5 N
Frictional Resistance (N)	88.3 N

Figure 4.1.4.2.1 - Parameter Values for Preliminary Torque and Power Requirements

4.1.4.3 Net Propulsion Force Calculation

Once all resistances to motion are found, the net propulsion force can be calculated according to *Equation 2.1.2a*. Since F_p can be equated to the sum of the motion resistances as defined in Section 2.2, the condition for motion becomes when F_s exceeds F_p as calculated above. For this calculation, a tracked vehicle is assumed such that *Equation 2.1.2h* can be used. In addition, a ground contact area A of 0.08 m^2 is assumed, which estimates the track area with dimensions stated above (.216 x .356 m). The weight W represents the maximum expected board and rider weight of 883 N. Finally, the cohesion c and shearing angle φ for average snow in the United States [4] are used from *Figure 4.1.4.3.1* below. The max tractive force $F_{s,\,max}$ calculated is 380 N. However, a realistic calculation for tractive effort of a track must include an estimate for track slip which reduces the tractive effort. Realistically, however, the maximum tractive effort that can be developed by a tracked vehicle is not achieved. For this calculation, a slip coefficient of 0.8 is used to estimate the amount of the maximum tractive force that is applied to the terrain after track slip losses. Actual tractive force is calculated using *Equation 2.1.2i* to be 304 N.

Variable	Value	Units
c	1.03	kPa
φ	19.7	degrees

Figure 4.1.4.3.1 - Parameter Values for F_s Calculations

4.1.5 Minimum Motor Power and Battery Energy

The power requirement needs to enable the snowboard to develop the maximum tractive force on the snow and propel the device at or above the minimum speed requirement. Also, a power safety factor was included in the battery and motor selection process to compensate for potential mechanical and electrical inefficiencies.

The tractive force used in these calculations is $F_{s,\,max}$ as calculated in *Equation 2.1.2h* for a tread system with an 883 N load to be 380 N. This is an estimate for the force that must be supplied to the tread so that the tread can supply a force F_s (304 N) to the ground. The power estimate is then calculated in *Equations 4.1.5a* through *4.1.5c*, and energy requirement for one hour of continuous usage in Equation 4.1d.

$$P = V_{min} * F_{s,max} \quad (4.1.5a)$$

$$P = (4.5\ m/s) * (380\ N) \quad (4.1.5b)$$

$$P = 1710\ W \quad (4.1.5c)$$

$$E = 1710\ Wh \quad (4.1.5d)$$

4.1.6 Motor Selection and Initial Speed Reduction Calculation

The team selected our motor based on the power requirement calculated in *Equation 4.1d* and market research of existing motors of similar products. The power requirement calculated in *Equation 4.1d* above is 1710W. When searching for motors within the electric skateboard market, it was observed that most of the electric skateboard motors commercially available exceeded 1710W. After discussions with electric skateboard builders online, we learned that the 6374 series motors are popular, reliable motors for custom DIY electric skateboard builds. The Flipsky brand 6374 motors advertised 3500W of power and 190 kV; kV is no load motor rpm per volt. The formula for kV is shown below in *Equation 4.1.6a*, where *rpm* is the motor revolutions per minute and *V* is input voltage.

$$kV = rpm\ /\ V \quad (4.1.6a)$$

The input voltage for the 6374-motor mentioned above is 43.2 V. At 190 kV, this means that the max motor rpm calculated using *Equation 4.1.4a* is 8208 rpm. To see if this motor could meet our speed requirements, the drivetrain speed reduction and the torque requirement are needed. The torque requirement and drivetrain speed reduction calculations are shown here.

Using a 5.101” pitch diameter and the sum of the motion resistances calculated in section 3.3.3, the torque requirement can be found. The torque requirement can be estimated using Newton’s second law and the equation for torque of the drive sprocket, shown below in *Equations 4.1.4b-c*, where F_{dr} is the forward-moving force at the ground created by the drive sprocket.

$$\sum F = m * a \tag{4.1.4b}$$

$$T = F_{dr} * r \tag{4.1.4c}$$

Equations 4.1.4b-c can be combined along with the compaction resistance and incline gravitational resistance to form *Equation 4.1.4d*, which is then solved for torque *T* in *Equation 4.1.4e*, where *r* is the drive sprocket pitch radius, R_c is the compaction resistance, F_{fr} is the friction resistance and F_g is the incline gravitational resistance. All resistance values are in newtons.

$$\sum F = \frac{T}{r} - R_c - F_{fr} - F_g = ma \tag{4.1.4d}$$

$$T = (ma + R_c + F_{fr} + F_g) * r \tag{4.1.4e}$$

Our mass requirement of 90 kg is substituted for *m* in the equations above. F_{fr} is calculated using a 10% incline (5.73 degrees), the normal force of the device on an inclined plane calculated in *Equation 2.2b*, and the kinetic friction coefficient between a waxed ski and snow of 0.05 [10]. A kinetic friction coefficient is used in place of static because compaction resistance only occurs during motion through snow. The compaction resistance is calculated using *Equation 2.2.2c*. The incline gravitational resistance is calculated using *Equation 2.2a*. The acceleration is a team-defined input; for these calculations, we used an acceleration of 1.25 m/s^2, which corresponds to reaching our target speed of 4.5 m/s in 3.6 seconds. The torque calculated using *Equation 4.1.4e* is 16.6 Nm.

The flipsky 6374 3500W motor mentioned above has a stall torque of 8 Nm. Our battery, however, limited the torque this motor can supply to 3 Nm, which is discussed further in section 4.4 below. Knowledge of max motor torque allowed us to calculate the gear ratio required to meet our torque requirement, shown below in *Equations 4.1.4f-h*, where T_{req} is the torque requirement, $T_{motor,\,max}$ is the max torque this motor can supply, and *GR* is the required speed reduction.

$$T_{req} = 16.6\ Nm \tag{4.1.4f}$$

$$T_{motor,max} = 3\ Nm$$

$$GR = \frac{T_{req}}{T_{motor,max}} \simeq 5.5$$

Thus, the drivetrain must include a speed reduction of about 5.5:1 to meet our torque requirement. Using gear sizes commercially available, the team was able to select gears that create a speed reduction of 96:17, which is approximately equal to the speed reduction calculated in *Equation 4.1.4h*. This speed reduction calculation is later refined based on the electrical limitations of our battery.

Knowing the speed reduction required if this motor was selected, we can estimate the max speed our motor can achieve using the motor speed of 8208 rpm from *Equation 4.1.4a*. This is shown in *Equation 4.1.4i* below, where S_{dr} is the revolutions-per-minute of the drive sprocket. This estimate is later re-analyzed using an empirical motor curve derived by an owner of an equivalent motor.

$$S_{dr} = \frac{8208\ rpm}{GR} \qquad (4.1.4i)$$

The drive sprocket speed calculated with *Equation 4.1.4i* is 1490 rpm. Using the pitch diameter of the selected drive sprocket of 0.13m (5.101”), we found the equivalent velocity at the ground to be 5.1 m/s (11 mph), which is greater than our target speed requirement. Therefore, the team selected this motor for use in our drivetrain.

4.1.7 Transmission

For the transmission, gears were selected over a belt drive. Belt drives are traditionally used with the motor we selected on electric skateboards with a ratio of 2:5 [61]. Because of the additional forces our system had to develop, our device needs a transmission ratio of over 2:11, which is further discussed in section 4.4.1. We rejected a belt drive because of space concerns and material concerns. Belt drives require spacing between the driver pulley and the follower pulley, this space would require the motor to be further back requiring redesign of the structural elements of the chassis. A gear system on the other hand would not require this spacing and the follower gear can be larger, which allows for a larger speed reduction. The other major reason a belt drive was not selected was that the belt itself would change material properties under the large operational temperature range, so it would not operate the same at lab temperatures and at below -6 ℃. Rubber belts tend to deform under cold temperatures and become brittle, and if our transmission failed it would halt all use of the device similar to a flat tire, but harder to replace. As Metals gears do not change under our expected temperature range, and they are able to be larger and not require more space for the transmission they were selected. A diametral pitch of 24 teeth per inch and an exact ratio of 17:96 was selected as it fit well inside the designed space for the transmission and still provided strong enough teeth so they would not shear, the

calculation for which can be found below. A prime odd number of teeth was selected for the driver gear, as it prevented the same teeth from meshing often leading to unequal wear.

Due to pricing concerns and wanting to learn a new machine, the team elected to Wire Electrical Discharge Machine (EDM) the gears. Having found 1.5 cm aluminum stock, the team avoided paying for gears; if the team had to buy the gears from a distributor it would have cost over $120. The Wire EDM converts the stock into an electrode, whereas the wire is the other electrode, such that once a voltage is applied to the wire, it jumps to the stock, cutting away the material into the designed shape. The Wire EDM in Washburn is not well maintained, resulting in multiple instances of mechanical failure during gear manufacturing, although the team was able to create the gears. The gears mesh well except for a burr on the driver, which is labeled in *Figure 4.1.7.1*, because of time concerns. The team sanded down the burr to reduce its impact on the transmission.

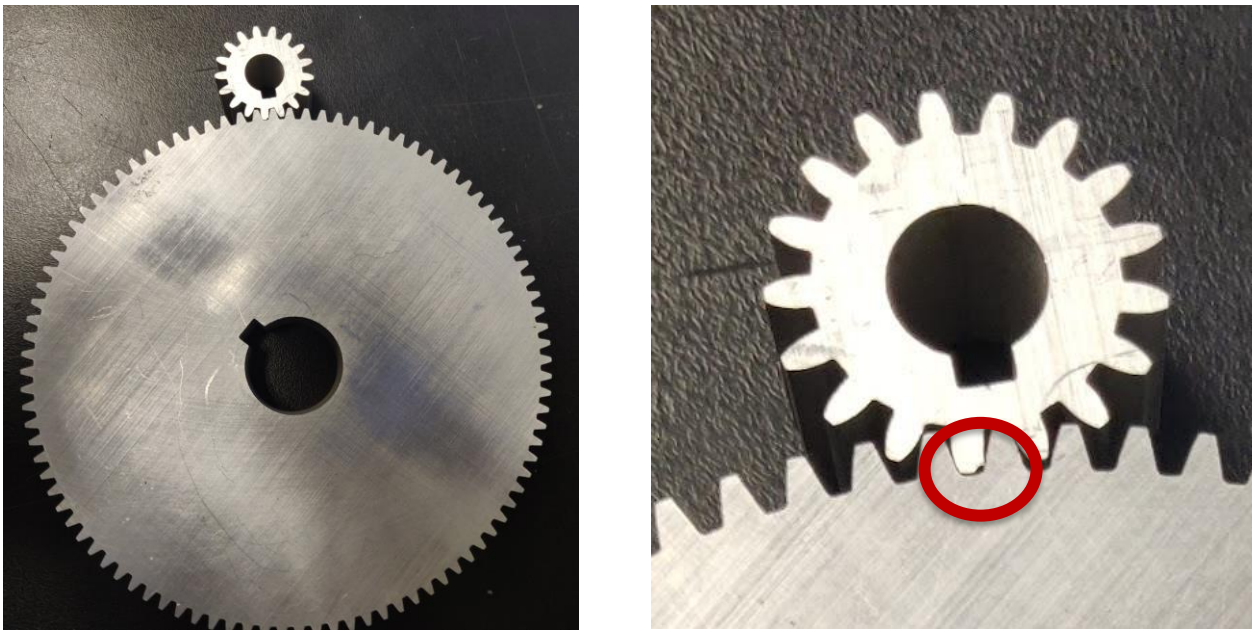

Figure 4.1.7.1 - Gear Mesh with Burr

Most gear teeth fail in one of two ways: tooth breakage from excessive tooth bending stress, and surface pitting from excessive contact stress on the tooth faces. Surface pitting can often be avoided with sufficient lubrication and the proper center-to-center spacing between mating gears. Tooth breakage due to bending stress on the gear teeth, however, required more detailed analysis. An analysis on the gear tooth strength was performed here to validate our design.

The bending stress on gear teeth was estimated using the Lewis equation for bending stress on gear teeth, as shown below in *Equation 4.1.7a*, where W_t is the tangential load on the

gear teeth in lbf, P_d is the diametrical pitch in in^{-1}, F is the face width in inches, and Y is the dimensionless Lewis form factor given by the corresponding chart shown in *Figure 4.1.7.2*.

$$\sigma_t = \frac{W_t P_d}{FY}$$

Equation 4.1.7a - Lewis Bending Stress equation for gear teeth [57].

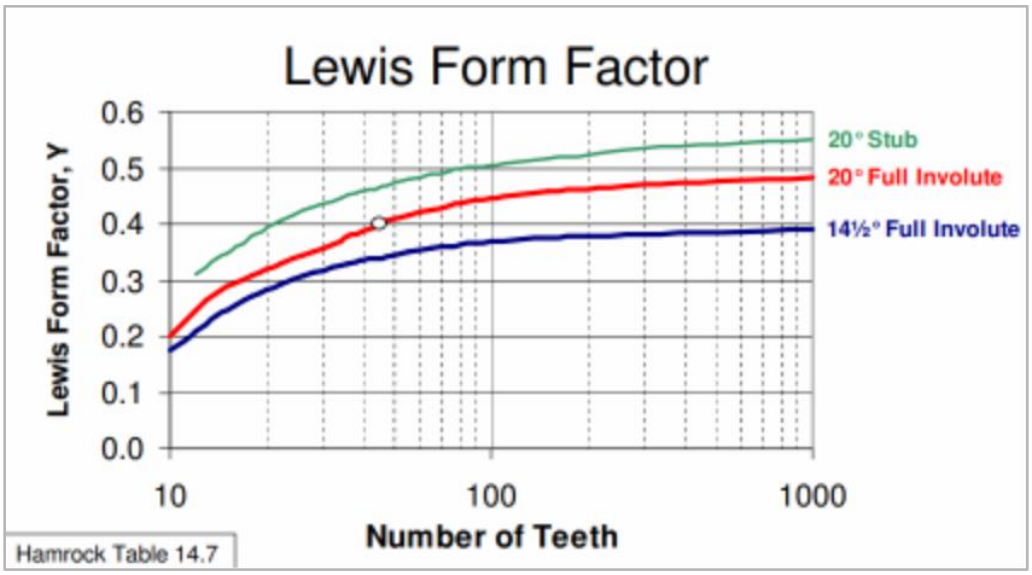

Figure 4.1.7.2 - Lewis Form Factor based on number of gear teeth and gear pressure angle [57].

The tangential load W_t was calculated using *Equation 4.1.7b* below, where T is the torque applied to the gear and d is the pitch diameter.

$$W_t = \frac{2T}{d}$$

Equation 4.1.7b - Equation for tangential load on gear teeth.

The team's first iteration of our drivetrain consisted of rigid gears with a 3:1 speed reduction. After additional calculation based on the output capabilities of our battery, this ratio was increased to 96:17, which caused the number of teeth on the driven gear to increase and that of the driving gear to decrease. The properties of our second-iteration drivetrain with this 96:17 gear ratio is shown in *Figure 4.1.7.3* below.

	Number of Teeth	Diametrical Pitch ($in.^{-1}$)	Face Width (in.)	Pressure Angle (deg)	Applied Torque (lbf-in)
Driving Gear	17	24	.5	14.5	70.8
Driven Gear	96	24	.5	14.5	400

Figure 4.1.7.3 - Properties of the team's second-iteration drivetrain gears. The "applied torque" of the driving gear is the anticipated max torque provided by the motor during stall.

The pitch diameter of both gears was then calculated using *Equation 4.1.7c* below.

$$d = \frac{N}{P_d}$$

Equation 4.1.7c - conversion from diametral pitch to pitch diameter.

The pitch diameter for both gears was then used in *Equation 4.1.7b* to calculate the tangential load W_t on both the driving and driven gear. The Lewis Form Factor was then estimated using *Figure 4.1.7.2* for both the driving and the driven gear. A Lewis Form Factor of 0.32 was estimated for the driving gear and 0.37 for the driven gear. Lastly, we used *Equation 4.1.7a* to calculate the bending stress on gear teeth for both gears. The bending stress was compared to the yield strength of the material used (aluminum 6061-T6) to estimate a safety factor for each gear design. The stresses and safety factors for both gears are shown below in *Figure 4.1.7.3*. Since the minimum safety factor is greater than 1, this design was deemed acceptable by the team.

	Bending Stress (psi)	Aluminum 6061-T6 Yield Strength (psi)	Material Strength Safety Factor
Driving Gear	30,000	40,000	1.3
Driven Gear	26,000	40,000	1.5

Figure 4.1.7.3 - Stresses and Safety Factors for Driving and Driven Gears

4.1.8 Drive Axle Strength Analysis

Because of the loads placed on the drive axle by the driveline gears, analysis was necessary to ensure the axle was strong enough to withstand these loads. Since the axle is attached on both ends to the frame, the load placed on the axle by the driveline gears can be approximated as a point load on a beam, as shown in *Figure 4.1.8.1* below.

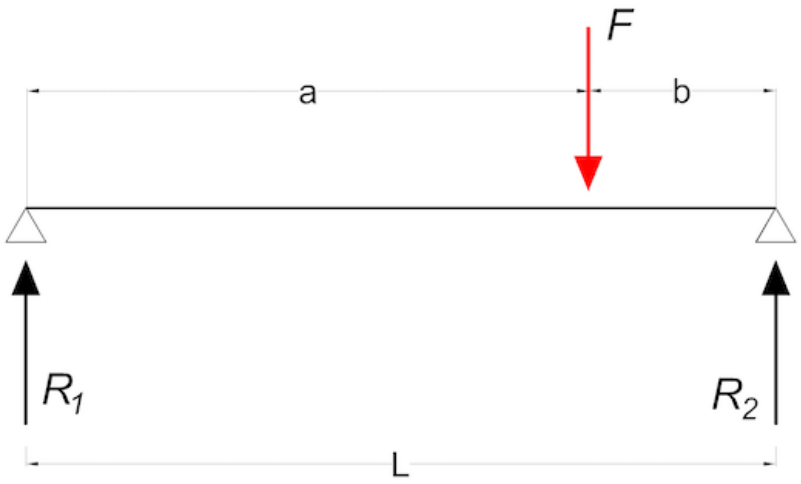

Figure 4.1.8.1 - Drive axle modeled as a beam supported on both ends under a point load.

Before the maximum stress in the axle can be calculated, the force F must be found. The force F can be described as the radial force F_r exerted by the driven gear in the drivetrain, according to *Figure 4.1.8.2* below.

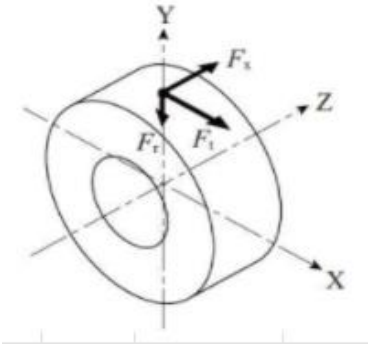

Figure 4.1.8.2 - Forces on a gear in a gear mesh. The force F_r is the radial force that pushes on the drive axle.

The equation for the force F_r is calculated using the torque T (Nm), the pitch diameter d (mm), and the pressure angle α (degrees) described by *Equation 4.1.8a* below, where the quantity $\frac{2000T}{d}$ is the tangential force acting on the gear.

$$F_r = \frac{2000T}{d} tan(\alpha)$$

Equation 4.1.8a - Equation for radial force F_r (in Newtons) of a meshing gear.

The force F_r is 396 N calculated with *Equation 4.1.6a* and the gear properties found in *Figure 4.1.8.2* above, which again uses the torque at stall for a conservative estimate.

Once the force F_r is known, it can be substituted for the force F in *Figure 4.1.8.1* above, and the maximum stress can be calculated. The maximum bending stress in the axle due to the radial load from the gear train is estimated using the equation for maximum bending stress in a beam supported at both ends under an eccentric point load, as shown below in *Equation 4.1.8b*. In the equation, y_{max} represents the distance from the neutral axis to the outer surface of the beam, F is the magnitude of the point load, a and b are the eccentric distances to define axial position of the point load, L is the total length, and I is the moment of inertia of the beam.

$$\sigma_{max} = \frac{y_{max} Fab}{LI}$$

Equation 4.1.8b - Equation for maximum bending stress in a beam under an eccentric point load.

A table of values used to calculate the maximum bending stress using *Equation 4.1.6b* is shown below in *Figure 4.1.8.3*.

Y_{max} (m)	F (N)	a (m)	b (m)	L (m)	I ($kg*m^2$)
.008	396	.064	.140	.203	.005

Figure 4.1.8.3 - table of values used to calculate max bending stress in the drive axle.

The maximum bending stress calculated using *Equation 4.1.6b* is 31.5 Pa, which is several orders of magnitude less than the yield strength of the steel drive axle (250 MPa). The team recommends a future MQP team reconsider the size and material used for their drive axle to save weight while still separating the maximum bending stress and the material yield strength with a safety factor.

4.1.9 Bearing Speed Analysis and Selection

The team selected bearings that both fit environmental device requirements and the necessary speed requirements. Sealed ball bearings were selected for rotating components, like the drive axle and sprockets, to prevent water or snow from damaging them. The team chose nylon bushings for use in the suspension system since the suspension components do not need to make full 360^{o} rotations, and they create little friction against metal surfaces. All ball bearings have maximum speed ratings. Because of this, the team calculated the maximum rotational speed expected for each rotating component where a bearing was used.

The rotational speed of bearings used for the drive axle, drive and idler sprockets were found with *Equation 4.1.9a*, where *rpm* is the bearing rotational speed in revolutions per minute, *v* is the linear velocity of the snowboard (in meters per second), and *d* is the diameter of the drive sprocket (in meters).

$$rpm = \frac{60v}{\pi d} \qquad (4.1.9a)$$

For the drive sprocket pitch diameter of 5.101” (0.1296 m), the bearing rotational speed can be calculated for both the target device speed of 4.5 m/s and the nice-to-have speed of 6.7 m/s. The bearing speed is 663 rpm using the target device speed and 987 rpm using the nice-to-have speed. The sealed ball bearings the team selected for use in the drive axle, drive and idler sprockets were sourced from McMaster Carr (part no. 6384K365) with a max rotational speed of 1,000 rpm.

The bearing selected for use on the motor shaft must endure the highest rotational speeds seen on the device. Using *Equation 4.1.4a*, the motor rotational speed under 43.2 volts is 8208 rpm. So, the team selected a sealed ball bearing that is rated for speeds more than 8208 rpm. The motor shaft bearing selected was also sourced from McMaster Carr (part no. 4390N148) with a max rotational speed of 15,000 rpm.

4.2 Chassis Design

The ground interface was designed to maintain the overall length of the board to prevent any added difficulty turning the board due to an increased length. To keep the overall length of the device similar to the original board, the rear of the snowboard was cut off and the chassis and tracks were placed in the space left behind. A low profile alongside an overall length of the system only about 20 cm longer than a snowboard, give the control and feel of a real snowboard. Two laser cut side panels are fixed together with five extrusion beams and hold three axles to form the chassis . The first is the steel drive axle, situated in the front, which is supported by bearings in aluminum housings which connect to the sidewalls. The next axle is the center axle, a dead axle, about which the entire chassis can rotate. The final axle, a dead axle in the rear which

the idler sprockets rotate about, is screwed to the sidewalls. In addition to the axles, there is a safety shroud, supported by stainless steel brackets, that doubles as a sled when you rotate the ground interface about the center axle. To tension the treads, a steel turnbuckle tensioner was placed between the center axle and the back axle. The computer aided design of the Ground interface can be found below in *Figure 4.2.1.1*.

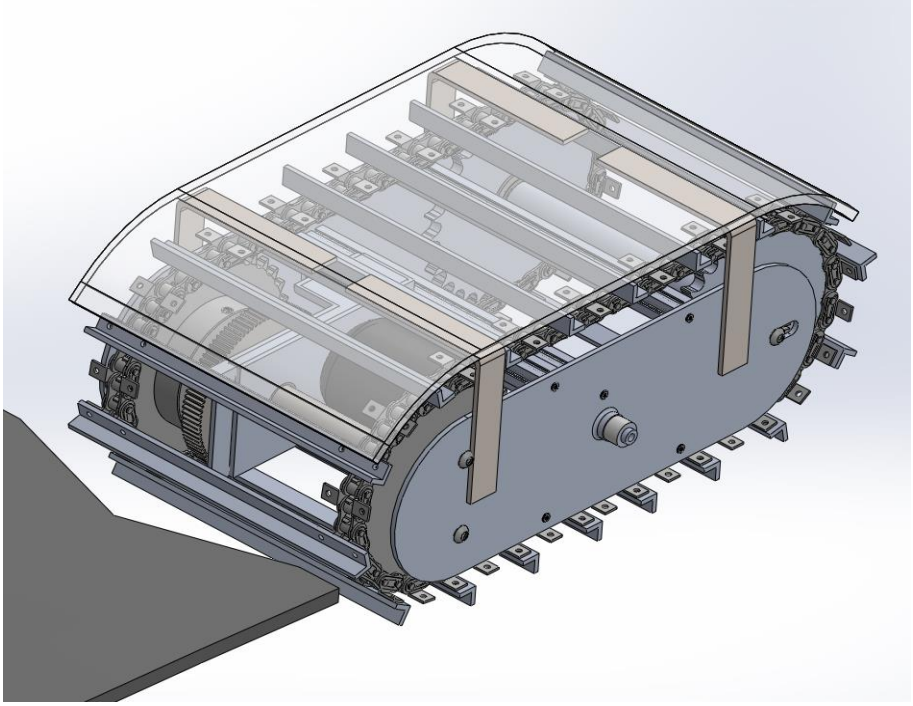

Figure 4.2.1 - CAD of the chassis

4.2.1 Material selection

Aluminum alloys were selected for most parts in our design because it is easily machinable, has a good weight to strength ratio and is easy to acquire. The technical requirement set in section 3 required the board to be under 245 N (55 lbf), to meet the requirements, the arms needed to weigh under 88 N (20 lbf) , which aluminum's density allows us to keep the weight low while still having strength in parts. Another important material property of aluminum is its strength, so with properly designed parts, the system will not buckle or bend under expected loads. Aluminum stock is also available in Washburn shops, alongside McMaster Carr, so it was easy to acquire stock to be machined. Furthermore, WPI's Washburn Shops have tools designed for machining aluminum available which reduces time required to machine aluminum.

Steel was implemented sparingly throughout the design to limit the additional weight. Steel is over twice as dense as aluminum, so it was selected mainly for fasteners, bearings, and the front axle, which support large loads. The cheapest non-uniform finished fasteners were selected throughout the design to reduce cost. The majority of the fasteners were imperial but the

screws which secure the motor to the motor mount were metric as the motor was designed using metric units.

4.2.2 Safety Shroud

The safety shroud is designed to protect the rider from both direct contact with the device and debris kicked up by the device. The safety shroud also serves as a sled to allow the user to ride the snowboard downhill, without resistance from the ground interface, when it is inverted. After researching, Polycarbonate and Ultra High Molecular Weight Polyethylene (UHMWPE) were selected as the main choices for making the shroud out of as both could support the loads and had different properties which made them advantageous. UHMWPE is used in snowplows to push snow; this is because it is slippery and when wet it becomes even more slippery. Polycarbonate was selected as it was easier to form into the correct shape. Polycarbonate can be thermoformed whereas UHMWPE would have to be machined, which would lead to much more waste material and require an additional time commitment. A combination solution was found, where we make the structure of the shroud out of polycarbonate and cover it with a thin sheet of UHMWPE to reduce the friction on the top surface of the shroud. Stainless steel brackets support the shroud. These were off the shelf parts with additional holes drilled to connect the shroud to the frame.

A finite element analysis was done on these brackets and the shroud to make sure that neither would break or bend when under the load of the device, fasteners and holes were left out of the analysis to increase speed. The load was applied to the shroud itself and the end faces of the brackets were fixed as they would not move in relation to the shroud. This was to simulate the ground interface impacting the ground uniformly with 120Ns or the weight of the ground interface and the suspension. The setup can be found in *Figure 4.2.3.1*.

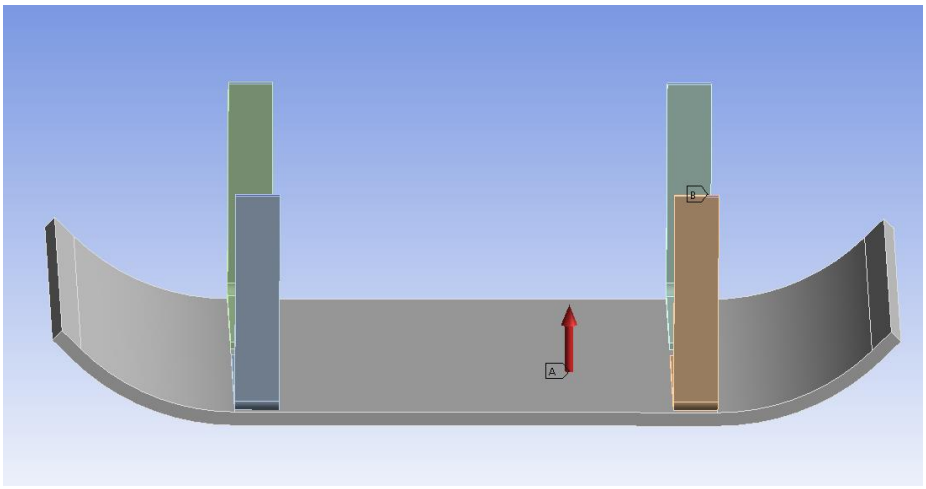

Figure 4.2.2.1 - Loading Conditions for Safety Shroud

The equivalent or Von Mises Stress study can be found in figure 4.2.3.2. The maximum values of this study were 2.3e+7 Pascals, which occurred in the bend of the arm brackets. The yield strength of the steel is 2.0e+11 Pascals, as the yield strength is over 1000 larger than the expected stress the arms will not fail, assuming the loading conditions previously laid out.

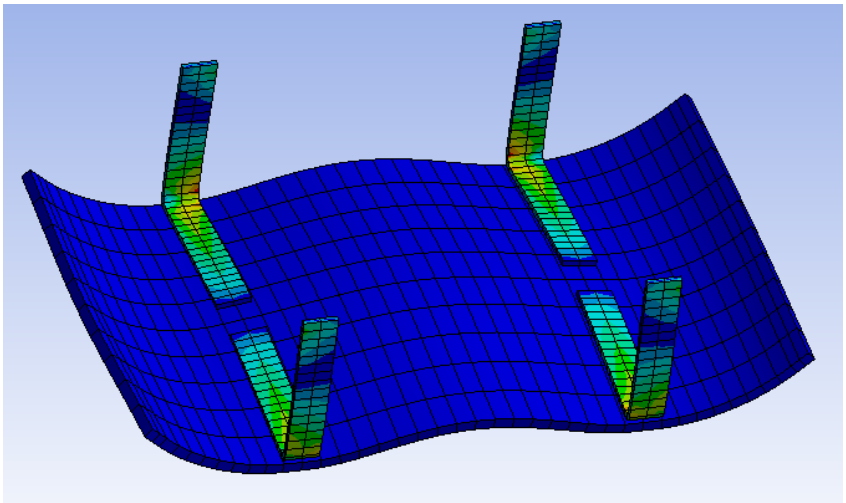

Figure 4.2.2.2 - Equivalent stress of the safety shroud

4.2.3 Tensioner

The purpose of the tensioner is to reduce slack on the grouser chains and keep them taught so they do not kink and cause problems around the sprockets or stall the motor. Originally the tensioner was a slot where the back axle can be pulled into the right location and the screws could be tightened to lock the motion along this slot, as seen in *Figure 4.2.4.1*. After basic testing of the chains, it was found this was not sufficient to counter the force the chain exerts on the back axle leading to slack in the chain. A turnbuckle used for tensioning rope was adapted to better tension the system. One of the turnbuckle's eye hooks is around the dead back axle and the other eye hook is cut off and a blind clearance hole was drilled halfway through the center axle to accept the tensioner. This alongside the slot allows for the back axle to be held in place when the chain starts spinning and can be found in *Figure 4.2.4.2*.

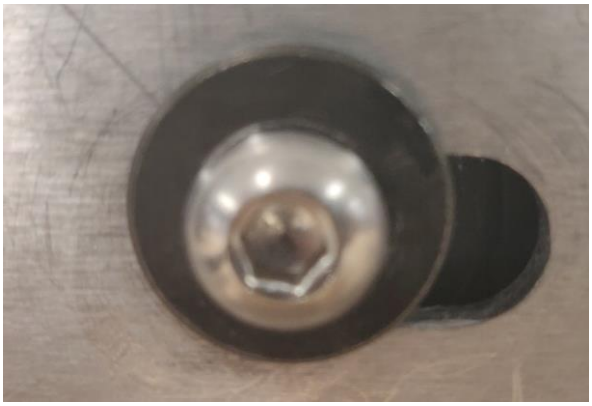

Figure 4.2.4.1 - Slot tensioner

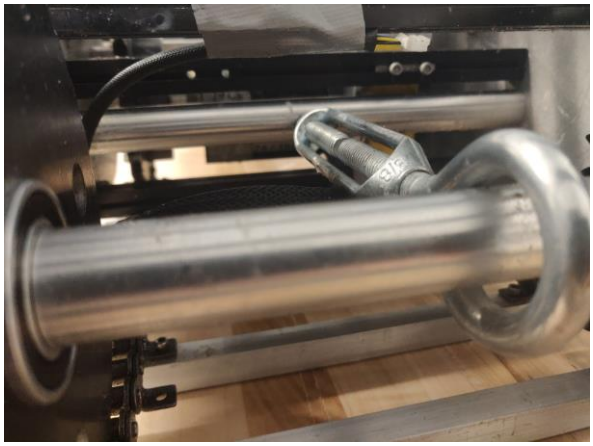

Figure 4.2.4.2 - Turnbuckle Tensioner

4.3 Suspension

Aside from the chassis and the drivetrain, the other major area of mechanical design is the method of connecting the chassis to the back of the board. The team generated the following criteria which would make a successful attachment method:

- Hold the ground interface in position behind the snowboard, touching the ground
- Apply sufficient vertical force to the top of the ground interface to develop traction given different snow types
- Allow the ground interface to translate and rotate relative to the board in desired axis to accommodate different snow types

During brainstorming, the “desired axes” of translation and rotation were discussed. Initially, vertical height adjustment and yaw rotation were desired between the ground interface and the board, as well as individual rotation of the ground interface, as shown in *Figure 4.3.1* below.

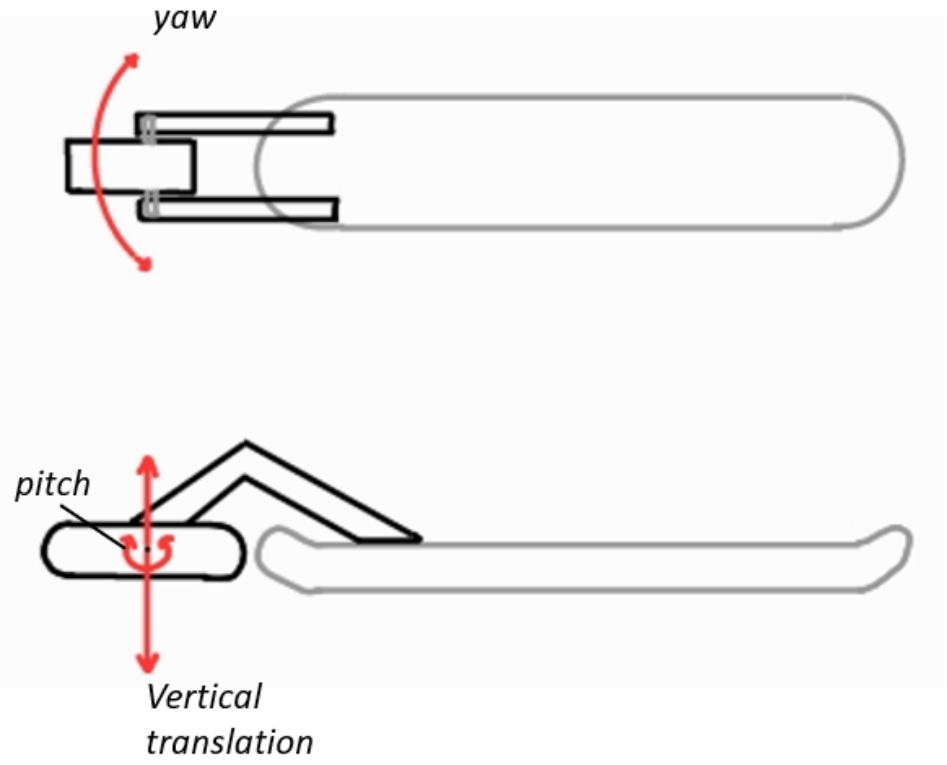

Figure 4.3.1 - Initial desired movement between the ground interface and the board.

Vertical height adjustment allows the rider to traverse both soft, deep snow as well as hard pack with the same traction. Height adjustment and individual rotation of the ground interface about an axis going through its center would allow the device to contour hills and valleys in the terrain without applying bending stresses to the arm material. Eventually, it was decided that only vertical translation and individual pitch rotation of the Ground interface (GI) would be feasible. Yaw direction motion of the GI relative to the board was desired, but for simplicity the concept was not favored. A thought proposed during brainstorming suggested using a similar mechanism to modern skateboard trucks to achieve yaw rotation between the GI and the board but was not realized. Including yaw direction rotation between the GI and the board was thought to reduce the effort required to negotiate a skid turn on the snowboard, freeing the rider from having to push the whole mass of the ground interface side to side during turning; thus, a future MQP might consider building this motion into a revised arm mechanism.

Accordingly, we found that a mechanism was needed to both pushes down on the ground interface to develop traction and allow for its vertical position to be adjustable. Before a mechanism was selected, calculations were performed to find how much vertical force should be placed on the ground interface to push it into the snow. Using equations from terramechanics literature, the thrust can be calculated of a particular ground interface [4]. The equation for thrust is shown here in *Equation 2.1.2h (repeated)*.

$$F_{s,max} = Ac + W tan\phi \quad (2.1.2h)$$

Equation 2.1.2h (repeated) - Thrust of a vehicle running gear, either a tread or tire [4].

The thrust in *Equation 2.1.2h (repeated)* is defined as a function of contact area, terrain cohesion and normal load. Increasing any of these three parameters (as defined in section 2.1.2. causes an increase in vehicle thrust; thus, a larger contact patch and/or a larger normal load placed on the ground interface would yield a greater tractive force on a given terrain, as long as the condition for flotation [calculated in Section 3.2.1] is maintained. Using empirical terrain parameters for cohesion and friction angle of medium-packed snow measured in Colorado, USA [4], the thrust of a ground interface with various contact area geometries and normal loads was calculated. Graphs of the *drawbar pull* (thrust) of a GI vs. the *weight on/of* a GI (normal load) are plotted below in *Figures 4.3.2 - 4.3.4.* For a 3"x6" contact area, the condition for flotation is not achieved when the load exceeds approximately 28 lbf (on *Figure 4.3.2),* and the sum of the motion resistances exceeds the drawbar pull of a given GI. The anticipated total maximum weight of the rider and system (250 lbf) was used as a conservative estimate to check for flotation, as calculated in section 3.2.1. During design, the graphs shown below were generated using imperial units to give the team members an intuitive feel for various ground interface sizes. However, we recognize that a consistent unit system is important for calculation uniformity and recommend converting all imperial graphs shown below to metric to match the established SI unit system in the future.

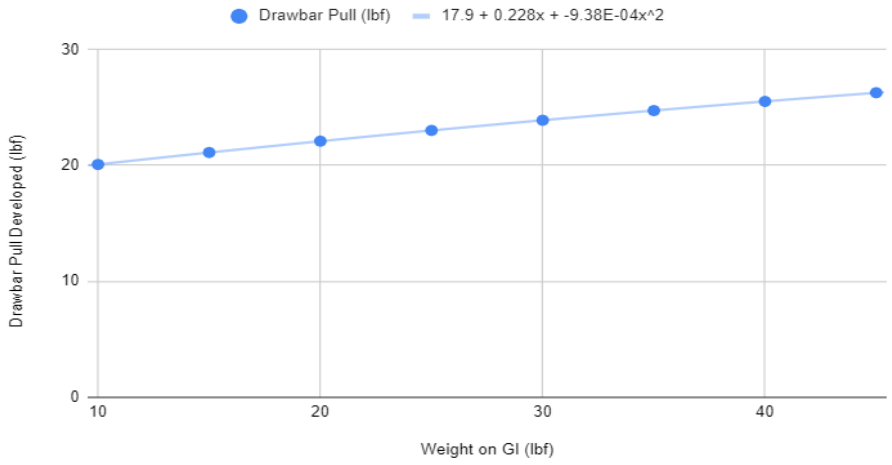

Figure 4.3.2 - drawbar pull vs. normal load on an 8.5"x14" ground interface.

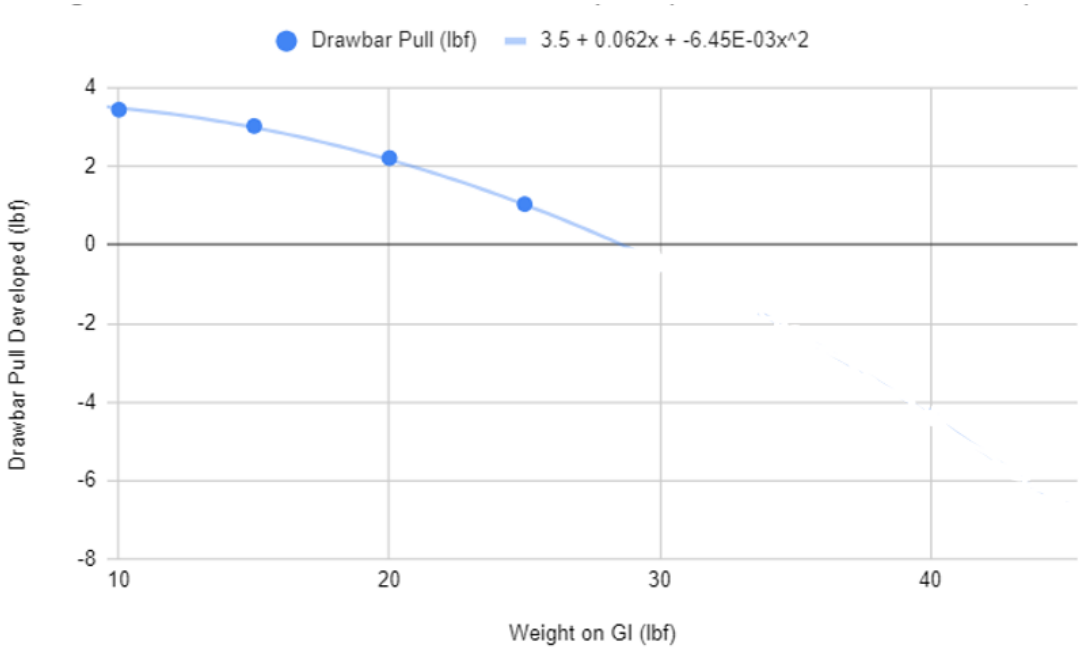

Figure 4.3.3 - drawbar pull vs. normal load on a 3"x6" ground interface.

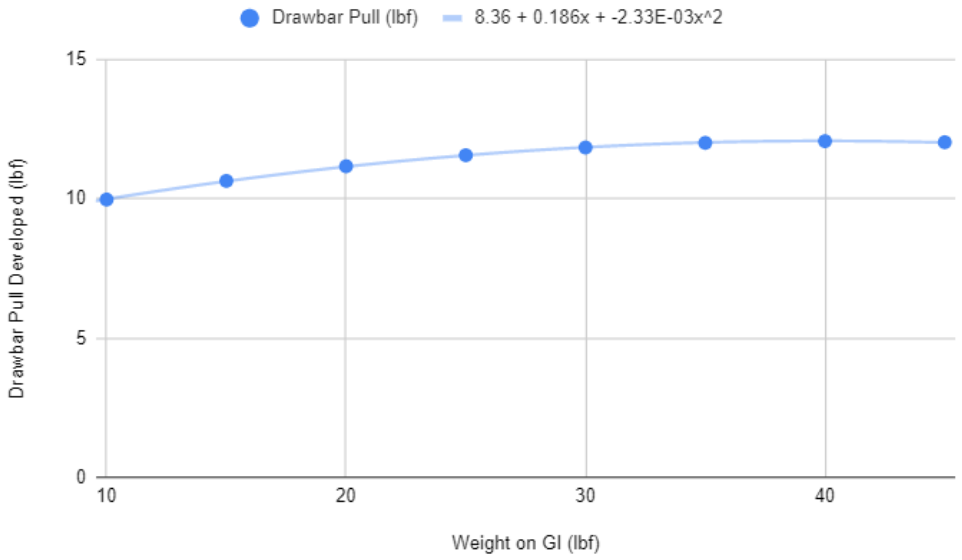

Figure 4.3.4 - drawbar pull vs. normal load on a 6"x9" ground interface.

To accommodate the length of the tread while keeping the entire device length similar to the original snowboard, we cut off the tail. This can be seen in *Figure 4.0.1.* To maintain similarity, a maximum length of 14" and a width of 8.5" was used in our design, whose calculated thrust is shown in *Figure 4.3.2.* It was found that the greater force that could be applied to the ground interface in the vertical direction, the larger tractive force the device could

generate. This vertical force would be applied as a combination of the ground interface weight and the vertical force applied by the suspension mechanism. During design, it was estimated from the 3D model that the ground interface may weigh a little less than 20 lbf. The estimated maximum acceleration of the device in snow could then be calculated using Newton's second law. This is done with the understanding that the drawbar pull of the GI is the net force after motion resistances are accounted for (compaction resistance and gravitational resistance assuming a 10% incline), and with knowledge of the device's mass. Using the established maximum total mass requirement (90 kg) and the drawbar pull calculated assuming 44.5 N of added vertical force (10 lbf) applied by the arm mechanism, it was estimated that the device could accelerate to a velocity of 6.7 m/s (15 mph) in 7.2 seconds. This is described by *Equation 4.3a* below.

$$F_{draw} = ma$$

$$F_{draw} = m \times \frac{\Delta v}{t}$$

$$\frac{\Delta v \times m}{F_{draw}} = t \qquad (4.3a)$$

As this maximum acceleration was deemed acceptable by the team, 44.5N (10 lbf) of vertical force applied by the suspension mechanism was favored. The maximum vertical force that could be applied to this contact area geometry before sinking was calculated to be 165 N (37 lbf) assuming the GI weight of 89 N (20 lbf), so there is ample room to exceed the 44.5N vertical force before motion is inhibited.

Originally, the design relied on torsion springs to push the arms around an axle and into the snow. However, after the vertical force calculations were performed, it was found that the torsion springs could not supply enough torque about the arm axle to supply the ground interface with the desired vertical force in the limits of reasonable size. As a result, we designed different iterations with a linear spring. During detailed design, the mechanical team brainstormed several potential mechanism concepts. Sketches of these mechanisms are shown below in *Figure 4.3.5 - 4.3.7*.

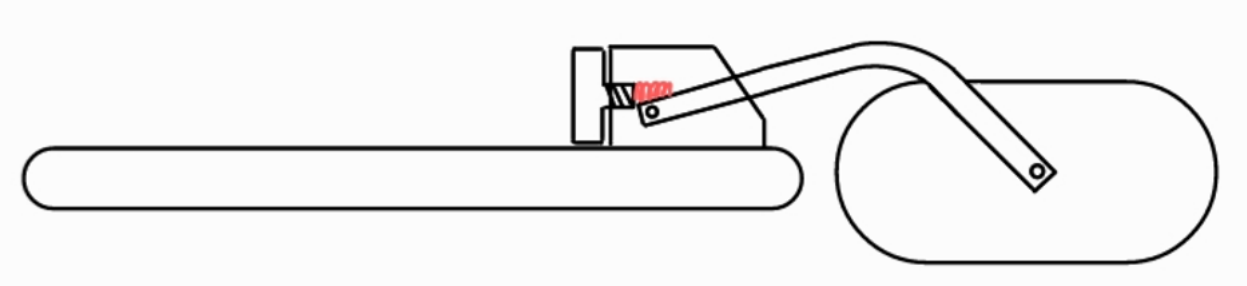

Figure 4.3.5 - Arm rotation mechanism concept using a linear compression spring.

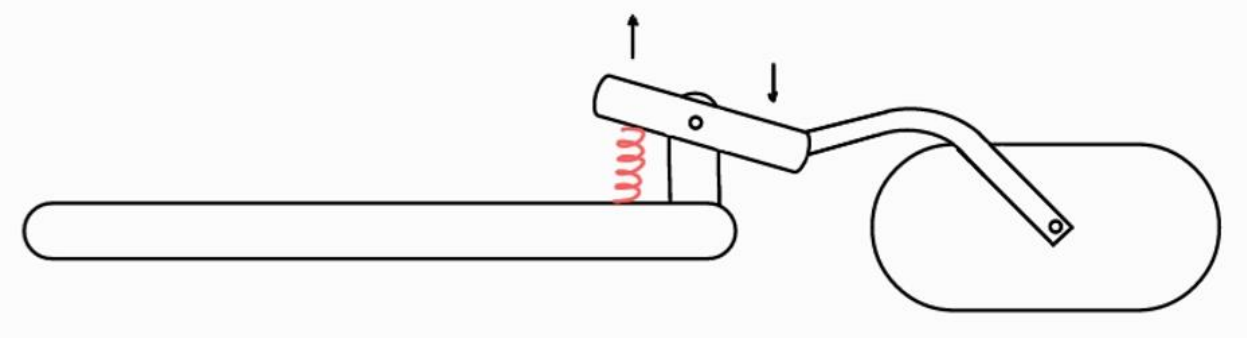

Figure 4.3.6 - Arm rotation mechanism concept using a linear compression spring and linkage.

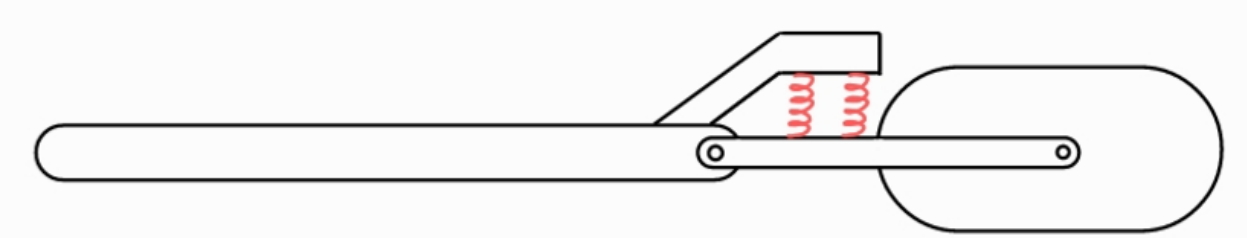

Figure 4.3.7 - Arm rotation mechanism concept using linear compression springs.

Several of the mechanisms used linear springs to push the arms about a pivot axle, forcing the ground interface into the snow. However, linear springs that push on a surface that rotates will deflect radially unless the spring rotates about the same pivot, as shown in *Figure 4.3.8.*

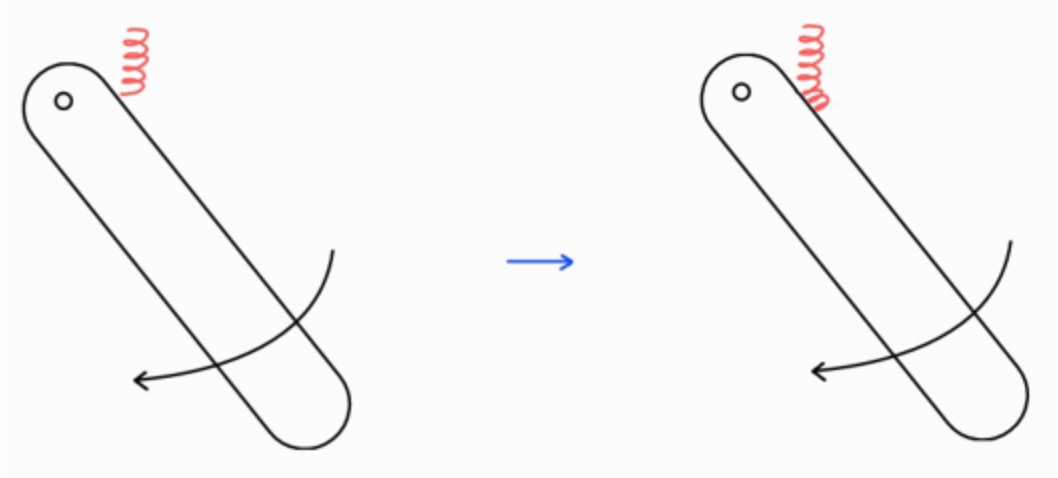

Figure 4.3.8 - Undesired spring deflection anticipated when a linear spring is used to push a rotating component. Linear springs must maintain perpendicularity with their contact surface.

Because springs deflect this way when pushing against a rotating link, we decided to create a linear-to-rotational mechanism to avoid it. In addition, both the vertical position and the amount of vertical force on the ground interface were required to be adjustable. The final mechanism that was selected was a modified crank-slider mechanism, as shown below in *Figure 4.3.9*.

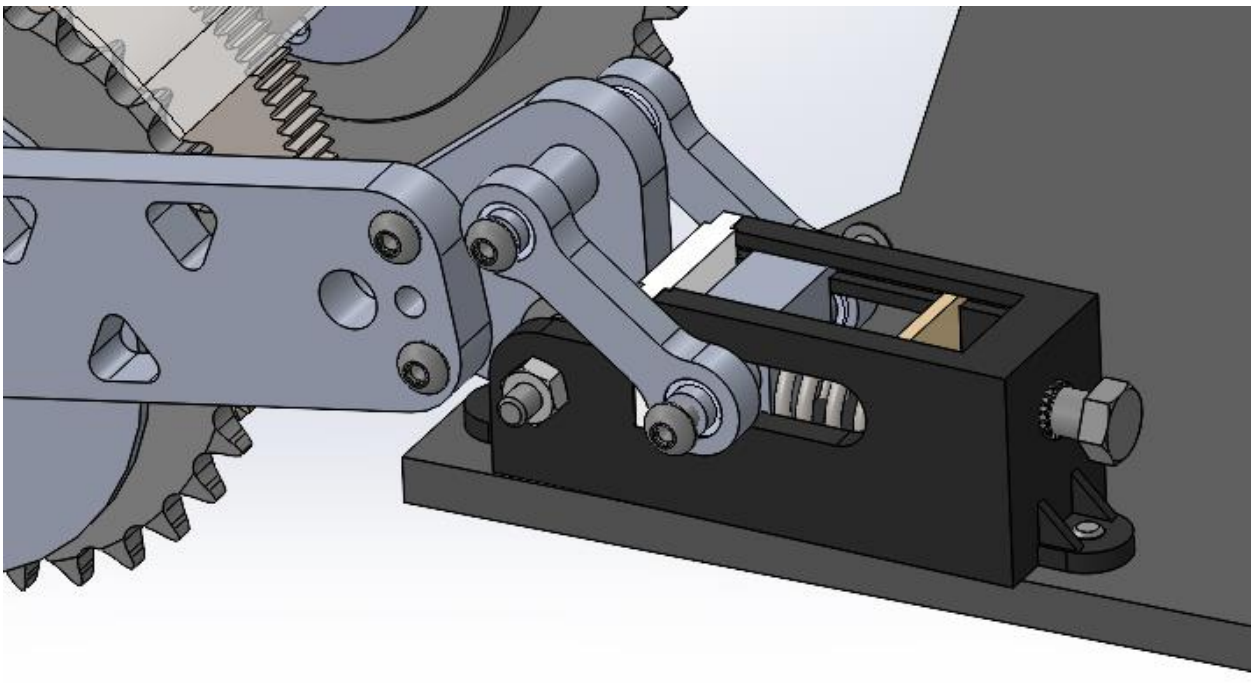

Figure 4.3.9 - First Iteration of modified crank-slider suspension mechanism

This mechanism featured sliding links that translated through a slot when pushed on by a linear spring. The neutral position of the spring could be adjusted by turning a hex bolt into or out of a threaded insert in the bracket front wall. In doing so, the spring would exert a variable amount of vertical force on the ground interface to be adjusted for different snow conditions. In deeper, more dry snow where the ground interface should sit lower in the snow to develop traction, the bolt could be tightened to push the arms further around their pivot point. In addition, any bumps the user hit while riding could be accommodated by the same linear spring acting as a suspension.

To achieve the drawbar pull of 107N (24 lbf) and the acceleration calculated in *Equation 4.2a*, 44.5N (10 lbf) must be supplied by the suspension mechanism. Thus, a spring had to be selected to achieve a total of 22.25N (5 lbf) per arm. The free-body diagram of the isolated arm mechanism is shown below in *Figures 4.3.10 - 4.3.12.* Note that the track is only included in the diagram to create a less abstract drawing. The units are intentionally left in imperial units because the manufacturer data for spring constants are given in imperial units. The desired vertical force applied by each arm mechanism to the terrain (the normal force in the y-direction) will be 5 lbf for a total of 10 lbf. This implies that F_{ny} = 5 lbf in *Figure 4.2.10* below. The tractive force of the device will create a reaction force on point a if the device is accelerating. The analysis below assumes the device is moving at a constant velocity such that F_{nx} is zero, and that the links are massless.

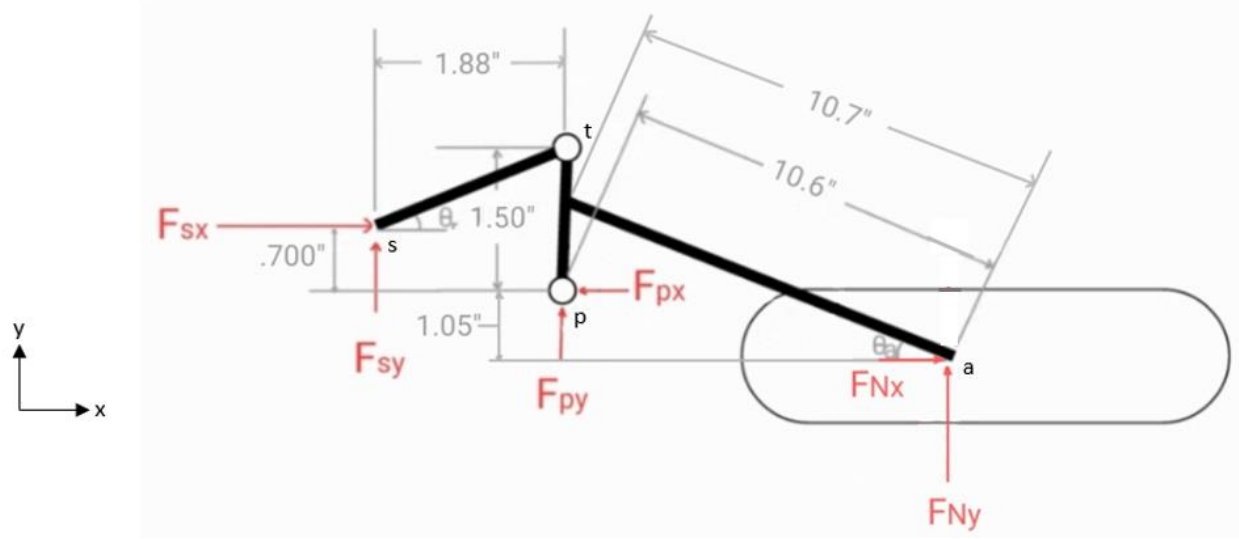

Figure 4.3.10 - Free-body diagram of the final crank-slider mechanism.

The force *Fsx* represents the spring force applied by the compression spring. and the angle θ_r represents the angle of the connecting rod relative to the spring. This FBD was broken up into two pieces to aid in solving. The first FBD is shown below in *Figure 4.3.11.*

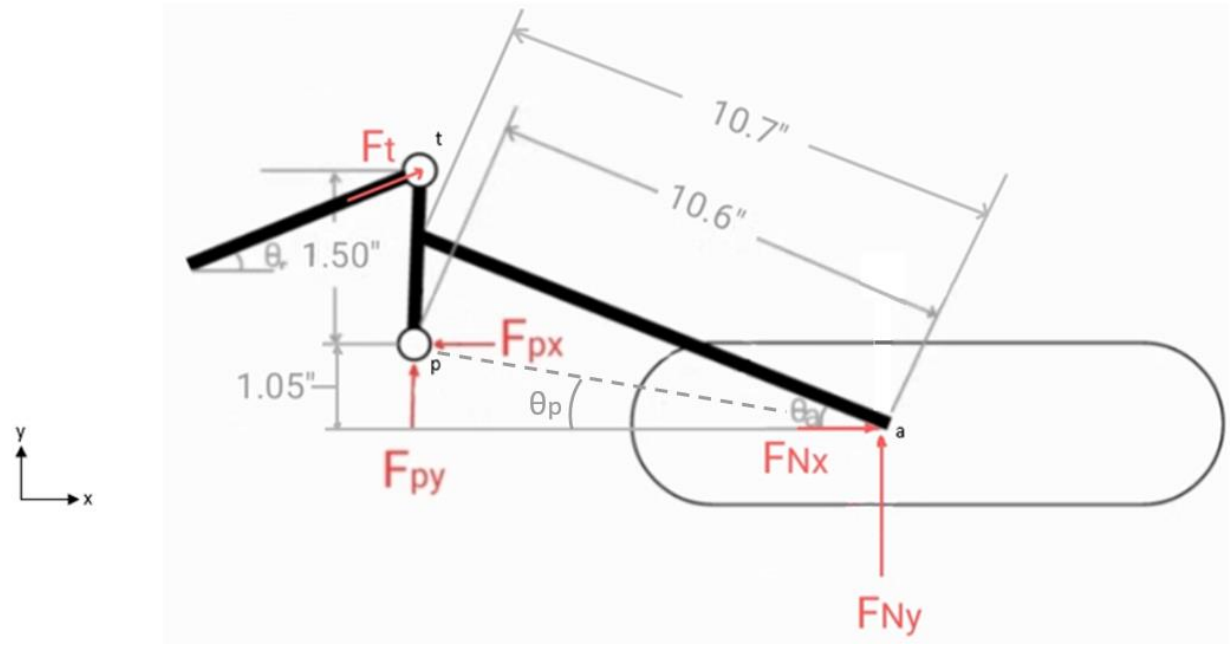

Figure 4.3.11 - First of two free-body diagrams used to solve for the required spring force Fsx.

The solution process to find *Fsx* involved first solving for *Ft* in *Figure 4.3.11* and then solving for *Fsx* in *Figure 4.3.12* below.

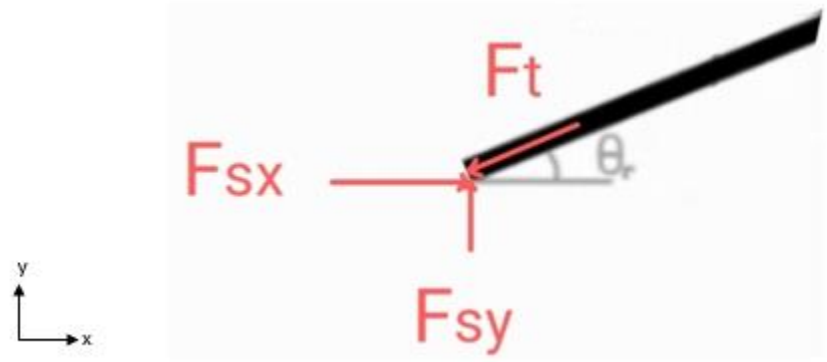

Figure 4.3.12 - Second of two free-body diagrams used to solve for the required spring force Fsx.

The solution process to find *Fsx* is shown below. The global variables are defined as follows: θ_p = 6.62°, θ_r = 23.1°, θ_a = 8.94°, and F_{ny} = 5 lbf. These are repeated for clarity in the solution process below.

Global Variables

$$\theta_r = 23.1°$$
$$\theta_a = 8.94°$$
$$\theta_p = 6.62°$$

Auxiliary Equations:

$$F_{ny} = 5\ lbf$$

Connecting Link and Arm FBD

Goal: Solve for F_t

$$\sum F_x = 0 = F_t cos(\theta_r) - F_{px}$$
$$\sum F_y = 0 = F_t sin(\theta_r) + F_{ny} + F_{py}$$
$$\sum M_p = 0 = 10.6cos(\theta_p)\, F_{ny} - 1.5F_t cos(\theta_r)$$
$$F_t = \frac{10.6cos(\theta_p)\, F_{ny}}{1.5cos(\theta_r)} \Rightarrow 38.2\ lbf$$

Arm bracket and Connecting Rod FBD

Goal: Solve for F_{sx}

$$F_{sx} = F_t cos(\theta_r) \Rightarrow 35.1\ lbf$$

The spring force F_{sx} was found to be equal to 35.1 lbf. This uses the input variables for θ_p, θ_a and F_{ny} as defined under the "Global Variables" and "Auxiliary Equations" headings in the above solution process. Once the required spring force was found, various off-the-shelf springs were compared to see which could supply the required force within their maximum rated deflection. The final spring, we selected has a spring constant of *k = 210 lbf/in*. This spring has a maximum deflection of *0.6 in*. The calculation for the required deflection for this spring is shown below.

$$F_{sx} = kx$$

$$k = 210\ \frac{lbf}{in}$$

$$x = \frac{F_{sx}}{k} \Rightarrow 0.167\ in$$

Since the required deflection of 0.167" is within the spring's maximum, this spring was selected for use in the suspension mechanism.

The mechanism shown in *Figure 4.3.9* required some redesign and improved materials choices for its components, considering the required spring force calculated above. The initial

arm bracket was a 3D-printed part, with a wooden sliding link in its slot. The threaded insert was a press-in insert which would be pushed into the plastic. Since the forces in the mechanism could very likely exceed the yield strength of 3D-printed plastic or the wooden sliding link, different materials for these components were desired. In addition, the threaded insert pushed into the plastic could have very likely sheared out of its mounting hole. After redesign, a mechanism was generated using a steel arm bracket, a machine tapped front wall, and aluminum sliding links. This is shown below in *Figure 4.3.12.* This mechanism also raised the vertical position of the line of action of the spring such that the angle theta in *Figure 4.3.10* was smaller. The final angle based on half of the rated max compression of the spring was 23.1 degrees, as opposed to 34 degrees in the design shown in *Figure 4.3.9*. Thus, the new mechanism utilizes a greater portion of the spring force available.

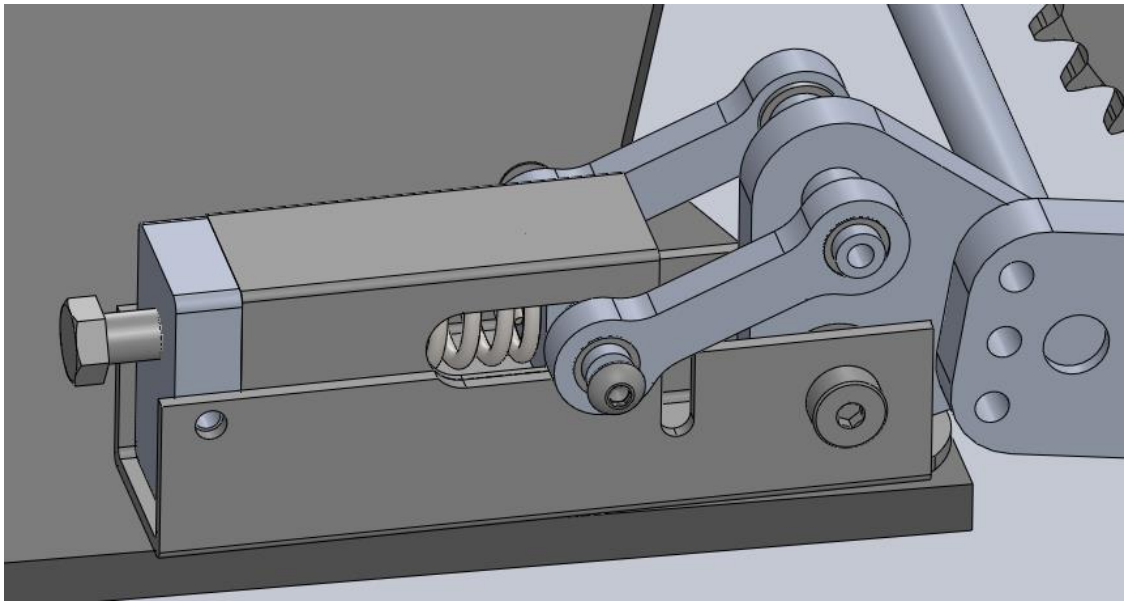

Figure 4.3.12 - Final design of the arm suspension mechanism.

4.4 Electrical Systems

4.4.1 Determining and Programming the Motor Controller

The motor controller was selected based on the motor specifications, the controller needed to have a higher peak current and voltage than the motor stall current and recommended operating voltage, which are 90A and 60V. The controller we purchased has a 100A peak current and operates at max 60V from Flipsky. In addition, the controller supported all the features needed, including, throttle curve adjustment, customizability using the VESC-tool, and connectable to an Arduino which we used to monitor the system (Section 4.6). Lastly, the motor controller was relatively inexpensive compared to the alternatives such as the Trampa brand VESC. With the motor controller and the motor selected, the next step was determining the required battery specifications.

The VESC uses a software tool, the VESC-tool, to set the specifications as well as set the communication type with a remote, and throttle curves for the motor. The main task was configuring the controller for a specific set of electrical components, mainly the battery and motor. Most of the settings were left in the default states except for the communication method (Section 4.6.2), and the specifications of the motor and battery. Regarding the motor, the VESC only required the type and weight of the motor, in this instance our motor fell under "the Outrunner Medium" category. In configuring the VESC for the battery, the required specifications included, the nominal voltage, max continuous amperage, cut off voltages, and max regenerative braking current.

4.4.2 Determining Battery Specifications

The motor we selected defined the battery we needed to satisfy the requirements of the device. The main requirements for determining the battery were a battery life of 1 hour and the battery weight cannot cause the device to exceed the maximum device mass requirement of 25 kg. In addition, the VESC has a maximum voltage of 60V and maximum continuous current draw of 50A. Also, the battery has size constraints because it had to fit within the area on the snowboard between the bindings as we determined that was the best spot to place it. These constraints helped narrow down the battery options, however, we still needed to ensure that the battery could supply enough power to push the rider. Since the battery life requirement specified on flat ground, the tractive effort was calculated using *Equations 2.2.2c*, for compaction resistance, and *2.3g*, for minimum tractive effort on flat terrain (repeated below).

$$R_c = \frac{1}{(n+1)b^{1/n}(k_c/b + k_\phi)^{(1/n)}}\left(\frac{W}{l}\right)^{(n+1)/n} \tag{2.2.2c}$$

$$F_P = R_C + \mu_{Board} W \tag{2.3g}$$

The required torque for traversing flat ground was then determined from multiplying the tractive effort by the drive sprocket radius of 0.065 m. The next step was looking into the ideal gear ratio to minimize the battery capacity required to satisfy the battery life requirement.

With the flat ground torque, we could determine the ideal gear ratio that resulted in the lowest required battery capacity without exceeding the size constraints of the ground interface or the motor stall torque. To determine this, we set up a spreadsheet to calculate the required motor torque given various gear ratios (*Figure 4.4.1*). The motor torques were then converted to motor current draw using the motor curve chart for the Flipsky 6734 190 kV motor (*Figure 4.4.2.1*). With our initial weight requirement of 1112 N (which assumed a 90kg rider and 25 kg board), the smallest capacity battery we could achieve was 30 Ah with a gear ratio of 1:6. When searching for potential batteries to use, we found that the ones with 30 Ah often failed to meet one more requirement (weight, size, or cost) or were not in stock. To reduce the capacity required, we determined the required voltage increase to maintain the electrical power of the motor using *Equation 4.4.1a*. However, the required voltage to reduce the capacity to 20 Ah was 57 V which would mean that the battery would operate for extended periods of time above the

maximum voltage of the VESC. Originally, our weight requirement was 1,112 N which allows for a 90 kg rider. Ultimately, we reduced the weight requirement to 889 N so our team members could still ride it. Then we tested gear ratios until we found that the smallest 30 V battery capacity, we could achieve was around 25 Ah with a gear ratio of 1:6. Again, we determined the required voltage increase to decrease the capacity while maintaining the same electrical power for the motor and remaining under the VESC maximum voltage rating. To note, the current and battery capacity are interchangeable, in this instance, because the battery life requirement is 1 hour.

$$\frac{I_1 V_1}{V_2} = I_2 \qquad (4.4.2a)$$

In *Equation 4.4.2a*, I_1 and V_1 are the given current and voltage (25 A and 30 V) based on the motor chart and I_2 and V_2 are the desired voltage and current (I_2 = 20 Ah).We found that with a 47.5 V battery we could reduce the required capacity to below 20 Ah while maintaining the gear ratio of 6:1. However, 47.5 is not a standard battery voltage so we rounded up to 48 which afforded us the ability to reduce the gear ratio further to the final gear ratio of 5.6:1 or 96:17. The final battery specifications based on the gear ratio, motor, and design constraints was a 48 V 20 Ah battery.

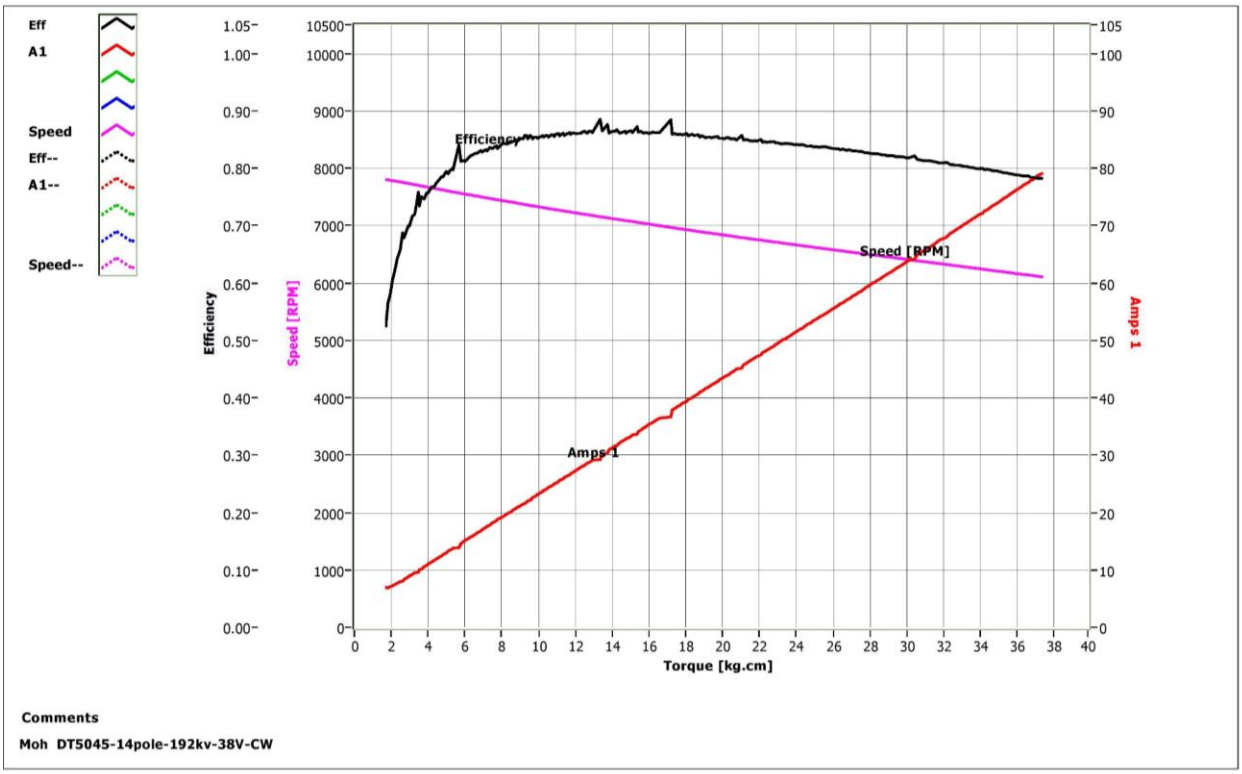

Figure 4.4.2.1 - Motor Curve Chart for Flipsky 6374 192 kV

Proposal Requirements:		**Units:**
Battery Life:	1	hr
Speed during BL:	7.5	m/s
Minimum Top Speed:	10	m/s
Construction Parameters:		
Drive Sprocket Radius:	0.065	m
Drivetrain Ratio	0.17	
Specs from Proposal:		
Minimum Required Tractive Effort	95	N
Minimum No load RPM	1447	RPM
Minimum Drivetrain Torque	6.2	Nm
Specs for Motor Curve Chart:		
Minimum Torque at Motor	1.05	Nm
Torque for Motor Chart	10.7	kgcm
Motor Voltage	38.0	V
Specs From Motor Curve Chart:		
RPM	7200	RPM
Efficiency	85	%
Required Battery Specs:		
Current (From Motor Curve Chart)	25	A
Battery Capacity	25	Ah
Current (manually calculated)	25	A
Battery Capacity	25	Ah
Actual Speed during BL:		
Drivetrain Ground Velocity	8.5	m/s
Required Voltage to Scale Current Down to 20 A:		
Scaled Up Voltage	47.5	V
Current Scale Down with 48 V:		
Scaled Down Current	19.79	Ah

Figure 4.4.2.2: Spreadsheet showing Results of Calculations that Determine Ideal Battery Specifications and Gearing Ratio

4.4.2 Battery Sourcing

Per the team's battery specifications, the power supply for the electric snowboard must be able to power a motor of 3.5 kW, maintain charge for more than one hour, fit within the 25 kg (55 lbf) total weight budget and be resistant to temperatures as low as -6℃. Ideally, a lithium ion (Li-ion) battery would be used in this instance as they are widely available and better suited for cold temperatures than other commercially available batteries such as lithium nickel manganese cobalt oxide (NMC) or lead acid batteries [50]. However, a lithium-ion battery would have to be custom ordered or built from individual cells by the team, which was not within the scope of the project [50]. The team ultimately decided on using a lithium iron phosphate battery (LiFePO4) found online as it fit all the specifications previously determined in section 4.4.1. A lithium iron phosphate battery is more cost effective, more durable, and safer than other types of batteries such as NMC or lithium nickel cobalt aluminum oxide (NCA) [50].

Upon searching for a battery to begin testing and electrical component layout, the team ran into some difficulty. We reached out to multiple custom battery vendors and found that a custom battery solution would not be cost effective for any of them and materials for batteries were more expensive due to pandemic induced supply shortages. Because the team had difficulty with online custom battery vendors, the team pursued local battery warehouses for a power source. Northeast Battery Supply in Worcester did not have any li-ion batteries in stock, and none of the products in the warehouse fit the board's weight requirement or were suitable for both cold temperatures [51]. Batteries Unlimited [52] in Worcester claimed that finding a 48V li-ion battery would be impossible, and that the best option to ensure the electric snowboard is adequately powered would be to create a custom battery. The store employee also advised against creating our own li-ion battery from cells as it could be dangerous, solidifying the decision to order a pre-built battery online.

To ensure that a battery found online met all the team's specifications, the team searched for batteries for similar applications, including electric skateboards or electric bikes. Electric skateboard batteries seemed promising as they are used for a similar application and come in a variety of capacities. However, electric skateboard batteries are rated for much lower voltage and current requirements than our specifications. This would have required us to purchase several electric skateboard batteries to power the device sufficiently. Unfortunately, the team did not have the budget to order several electric skateboard batteries and had to begin searching for other batteries. The team found the most promise in searching for electric bike batteries, as they met voltage, current, size and temperature requirements. Ultimately, the team decided to use a LiFePO4 battery from BtrPower designed to be used with an electric bike. The battery fit the specifications outlined in section 4.4.1, the team's budget, and came from a reputable source. Upon ordering and setting up the battery with the motor and speed controller, we determined that

the battery functioned as expected, and moved forward with testing subsections of the electrical system.

4.5 Software Systems

This device relied on the software and electrical systems to enable the user to control the speed and to know when the system encountered any issues. To control the speed, the user would press the right trigger on a wireless Xbox controller. That signal would get transmitted through Bluetooth to an Arduino mega which managed all the sensor data and controlled the safety features. The Arduino, if there is an issue, will tell the remote control to vibrate to notify the rider. To help the user determine the issue, there are notification LEDs that indicate the electric snowboard detected a rider, that the motor stalled, if the battery is within its operating temperature range, and if it is sufficiently charged. Assuming the device was operable, the Arduino would send the signal to the VESC which would command the motor to rotate. These systems all worked together to propel the snowboard per the user's command.

4.5.1 User Interface

Since the team wanted to use a wireless controller, a few requirements dictated the specifications to enable reliable control. The first is the remote needed to have a battery life as long if not longer than the device of the board, 1 hour. Secondly, the user needs to be able to control the device while wearing gloves. Third, the controller needs to withstand the cold temperatures expected while riding. Fourth, the remote needed to notify the rider when there was an issue. To determine the specifications to meet the requirements, we approximated a Bluetooth remote control's power consumption, including capacity loss due to the cold, to be roughly 285 mAh, based on parts listed in *Figure 4.5.1*. The battery life used for the power consumption is 1.3 hours to compensate for an estimated 30% capacity reduction [58].

Component	Current Draw (mA)
Arduino Nano	19 [59]
LED 2x	20 [60]
Bluetooth Module	30 [36]
Extra Peripherals (i.e., Vibration Motor)	40 [34] [35]

Figure 4.5.1 - Parts List of Electronic Components

With the specifications, we began looking for a remote control and found that there are none available with haptic feedback. This was crucial because we needed a way to alert the rider

without requiring visual feedback. Initially, we devised a method for audio feedback although the solution would have been potentially irritating for the user. Then we decided to look into video game controllers since they often incorporate haptic feedback. The team had an Xbox One wireless controller available which worked well for initial prototyping. With the controller, only an Arduino USB Host Shield and a USB Bluetooth dongle were required to control the device which was cheaper than other remote-control solutions. Also, there is a software library, USB Host Shield 2.0, that enables the Xbox controller to communicate with an Arduino through UART. To control the device, the user would simply press the right trigger to accelerate the motor.

4.5.2 Arduino Mega and USB Host Shield

To monitor the system and enable the custom control scheme, we needed to implement a microprocessor to manage it. Originally, we wanted to use only a VESC, but it lacked the capabilities required to monitor the system and interface with an Xbox controller. We needed another microprocessor to monitor various system parameters to ensure proper function and rider safety. To do so, we implemented the system software on an Arduino mega. We specifically chose an Arduino mega for its ease of use for prototyping and plethora of inputs and outputs. Arduino mega has multiple hardware serial connections which were required since both the VESC and the Xbox controller communicated through the universal asynchronous receiver transmitter (UART) protocol. The VESC also supports pulse position modulation (PPM) protocol, but it bypassed many features of the VESC and required calibration. In addition, the Arduino mega had ample digital and analog inputs and outputs for the multiple sensors required for the snowboard. *Figures 4.5.1* and *4.5.2* show the fully wired electronics box with the Arduino, VESC, and battery with the temperature sensors mounted on the sides, respectively.

A UML diagram of the software on the Arduino is in Appendix 6.C. In software there are two main classes, mcLED and analog Sensor along with the main file which contains the main control loop. mcLED was a class that controlled multicolor LEDs which notified the rider of the different states of the monitored snowboard parameters. The analog Sensor class read values from the pressure sensor and the temperature sensors used to monitor the battery temperature and rider detection system. In addition , the analog Sensor class implements some signal processing techniques discussed in section 4.3.5.4. The VescUart library, written by Solid Gecko, enables the VESC data to the Arduino regarding the battery and the motor. The Arduino relayed controller signals to the VESC using the same library. The USB Host Shield enabled the Arduino to communicate with the Xbox controller, as mentioned previously.

4.5.3 Notifications System and Sensors

Below is an image of the housing for the LED notification PCB which was mounted on the top of the device and alerted the rider of the snowboard parameters.

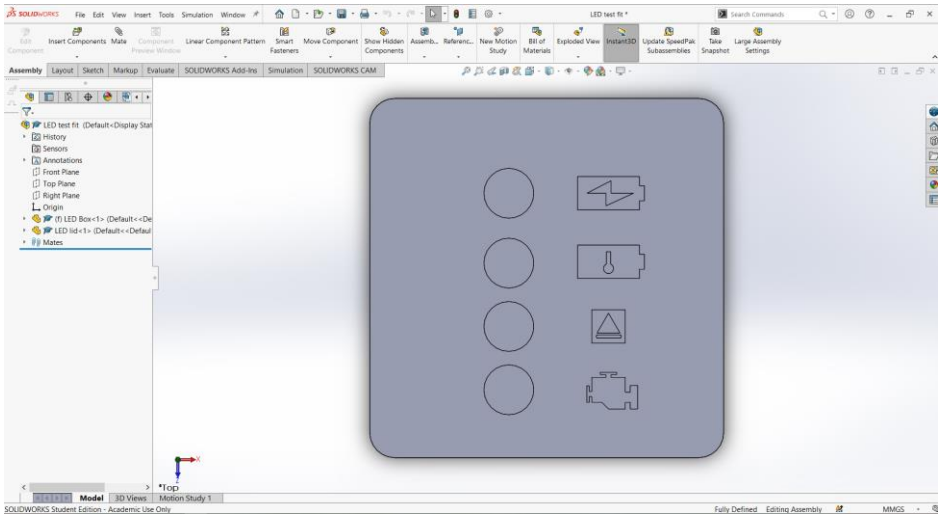

Figure 4.5.3 - Notification System Interface

The LEDs indicated four system parameters that determined device operability: whether the rider is strapped in, battery temperature, battery state of charge (SOC) and motor current draw. The LEDs are located on top of the electronics box between the two snowboard bindings. Whether the rider was strapped in, referred to as rider detection, was monitored by a force sensitive resistor pressure sensor installed in the front binding. Five TMP36 temperature sensors were attached to the battery to monitor the battery temperature. Battery SOC was transmitted from the VESC and determined if the battery has enough charge to run. Lastly, motor current draw was also acquired through the VESC and used to determine if the motor had stalled. Whenever the system detected an issue, the remote would stop spinning the motor and start vibrating when the throttle is pressed until the issue is resolved.

4.5.3.1 Force Sensitive Resistor based Rider Detection

To ensure the rider is strapped in, the team determined the need for some form of rider detection within the bindings of the snowboard. Originally, the team planned to incorporate a limit switch within the bindings that would close as the rider secured the bindings, but eventually deemed a limit switch as too bulky, and as having the potential to interfere with the binding. Ultimately, a pressure sensor was placed within the bindings to ensure the rider was secured into the bindings appropriately. The team budgeted for one pressure sensor within each boot but chose to include one pressure sensor. Using one pressure sensor instead of two allows the rider to remove one foot to propel themselves out of a rut, without the system stopping because it deems the rider is not secured to the board, snowboarders typically use their back foot to push off the snow in a technique referred to by snowboarders as skating. To determine placement of the pressure sensor the team measured readings from the sensor while it was placed on different sections of the snowboard binding boot used in the final prototype. The most consistent and

reliable readings were obtained when the sensor was placed on the underside of the bindings of the snowboard beneath the boot, as shown in the *Figure 4.5.3.1* below.

Figure 4.5.3.1 - Snow Packed into Baseplate of Snowboard Binding

Figure 4.5.3.2 - Rider Detection Sensors Placed Within Appropriate Location within Snowboard Bindings

The pressure sensor acts as a digital sensor, confirming pressure, or lack of within the bindings. As a result, a force sensitive resistor (FSR) is used to detect the boot strapped into the binding. This was simple to implement because FSRs have an inverse logarithmic relationship to the amount of pressure applied to the sensor. To read a value close to 0 volts, a rider would have to be safely strapped into the bindings with the sensor. One concern is that the FSR requires a voltage divider circuit. Because a voltage divider current requires resistors, and resistance decreases as temperature decreases, the use of a voltage divider sensor on a snowboard may not be reliable. However, this problem is irrelevant due to lack of accuracy required for rider detection. Another potential issue was that snow buildup in the bindings could cause the snowboard to think a rider is strapped in (*Figure 4.5.3.1*). Snow builds up in the bindings turned out to be a non-issue because FSRs typically need at minimum a 98.1 N weight in order to register any change in pressure. Another concern regarding the pressure sensor is the sensor reporting that the rider is not strapped in when they turn heel side or toe side, shifting weight off of the sensor, causing the motor to stop.

4.5.3.2 Battery Thermal Monitoring

Batteries discharge current at a reduced rate and have a reduced capacity at lower temperatures. Additionally, the battery cannot charge in cold temperatures without suffering lithium plating damage on the anode. Conversely, thermal runaway and subsequent bursts into flames result from batteries overheating. In either instance, the rider risks reducing the lifespan of the battery and subsequently the lifetime of the electric snowboard. For our particular battery, the appropriate temperature range for the battery is 15-35 ℃ [53]. To combat the issue of over or underheating, the temperature of the battery is constantly monitored during device use to ensure the device would not operate outside of the battery's ideal temperature range. Initially thermistors were to be implemented to measure the battery temperature as they were very accurate and inexpensive. However, thermistors do not function as accurately in cold temperatures because they rely on a voltage divider circuit with a fixed resistor. The main issue is that the impedance of a fixed resistor significantly decreases in cold temperatures, causing the reading on the thermistor to change. As a result, TMP36 temperature sensors were used instead, which did not require an external resistor, provided consistent readings, and functioned between -40 and 150 ℃ [55]. Implementation wise, TMP36 sensor change in voltage is directly proportional to change in temperature which is simpler than calculating the temperature from thermistors. Having found a suitable temperature sensor, five were mounted to the battery: one on each side except the bottom. Temperature values from each sensor are recorded and averaged to obtain a comprehensive estimate of the battery temperature and determine if the battery temperature was in the previously specified, ideal range.

4.5.3.3 Battery State of Charge

Batteries are rated by nominal voltage because the voltage is not constant while discharging the battery [56]. In our battery, for example, when it's fully charged the battery voltage would hover around 58 volts and when fully discharged the voltage is around 38 volts. The voltage curve at different capacity levels is best described as a cubic function were. When near fully charged or close to no charge the voltage changes rapidly while the voltage stays relatively constant in the middle. Generally, when LiFePO4 battery is less than 30% SOC, the voltage will begin to decrease rapidly which is when the rider needs to know the battery is at low charge. In our system, we set voltage thresholds at 44 and 48 volts to alert the rider when the battery is roughly at roughly 10% and 20% SOC respectively. When the battery is above 20% the battery SOC LED indicator is green, between 10% and 20% the LED is yellow, below 10% the LED is red. To protect from over discharging the battery, below 10% SOC, the device will not let the rider control the throttle. To detect changes in SOC, the VESC will relay the information to the Arduino. The VESC is also responsible for telling the Arduino the motor current draw for motor stall detection.

4.5.3.4 Motor Stall Detection

From initial research, a main concern regarding the device was the potential for the treads utilized by the drive system to stall. Snow could build up and could clog the drivetrain inside the tread system and cause the motor to stall. The fourth LED in figure # above indicates if the motor stalled and will change from green to red in such an event. To detect motor stall, the Arduino reads the motor current consumption from the VESC to use a proxy for the amount of motor torque currently being produced by the device. After a specific amount of time running the device at expected torque loads, if the device begins consuming greater than 80 A, then the motor is considered by the system to be stalling. To ensure the rider can safely remove snow from the treads, the device will be shut off while the motor stalled. Upon running the device again, provided the drive system is clear, the system will function as designed. This set up resulted in the ground interface jittering because the motor to stall it requires current. When the Arduino detects the motor has stalled, the motor stops, causing it to stop drawing enough current to indicate that it stalled. If the rider is holding the throttle down, this process would repeat, causing the jittering effect with the motor oscillating between drawing no current and stall current. To fix this in future iterations, power to the motor will not be stopped when the Arduino detects that the motor stalled, however, we will keep the haptic feedback to maintain the rider notification. With all the sensors, the Arduino had some trouble processing all the information.

4.5.3.5 Software System Issues

When reading multiple sensors simultaneously, specifically the temperature sensors, the readings were very inconsistent with each other. The inconsistency was a result of sensors competing for the ADC in the Arduino; each sensor would interrupt the ADC and prevent it from processing previously sent signals. As a result, the sensors would read values up to 10 °C apart

from each other despite being in the same room and having an accuracy of ± 1 °C. To solve this issue, the Arduino waits for a short period of time before reading a value then disregards that value, then reads then returns a second value. Another issue was that the sensors would often oscillate ± 1-2 °C, which could cause issues when approaching a threshold value. To resolve this, a moving average filter was implemented to reduce the oscillations. Both of these fixes as well as converting signals to appropriate units were implemented in the analog Sensor class. The entire software structure is shown in a UML diagram in Appendix 6.C.

4.6 Electronics Layout and Integration

Due to the nature of snowboarding, it was of utmost importance to protect the electronics system, motor and battery from cold temperatures and snow. To protect the electronics from the elements, the team opted for a waterproof junction box, which is typically used in industrial applications to protect commercial electronics. To accommodate the size of the battery, the box dimensions were 300 mm long, 200 mm wide and 170 mm tall(11’ long, 7.9’ wide and 6.7’ tall). Thus, large enough to fit the battery, which is 269 mm long , 154 mm long, and 93 mm tall (10.6’ long, 6.1’wide and 3.7’ tall), as well as other electronics, but small enough to fit between the bindings of the snowboard [54]. The case itself is waterproof, but in order to accommodate the power switch for the system, pressure sensor used in rider detection, motor wires and battery charging port, adding holes to the box was a necessity. To ensure the box remained waterproof, the external wires such as the motor power wires, and pressure sensor wires were wrapped in protective covers and secured to the box. Holes in the box were cut exactly to size, and 3D printed dummy plugs were added to ensure the box remained watertight and to protect the battery charging and power key ports.

Additional mounting hardware is necessary to secure electronic components within the box. Because the electric snowboard was outfitted with an Arduino, custom circuit boards for the LED notification system, pressure sensor, temperature sensors and VESC, the layout of the electronics system was completed with careful consideration. 3D printed mounting brackets were created to house the pressure sensor, custom LED notification system, and temperature sensors. All the 3D printed housing was designed for the custom circuit boards to be press fitted. Available space in the electronics box is limited due to size constraints pertaining to the battery and available space on the board. Thus, the prints to house the Arduino, protoboard busbar and pressure sensor are designed to fit with the VESC within the lid of the box. All the 3D printed housing for the boards mounted within the lid of the box are secured with glue, which protects the boards from adhesive and moving around during regular device use. The cases for the temperature sensor circuit boards are designed to hold the edges of the board in place to not interfere with the sensors or the wires connecting them to the Arduino and are shown below in *Figure 4.6.1*. The remainder of the circuit boards are shown below in *Figure 4.6.2*.

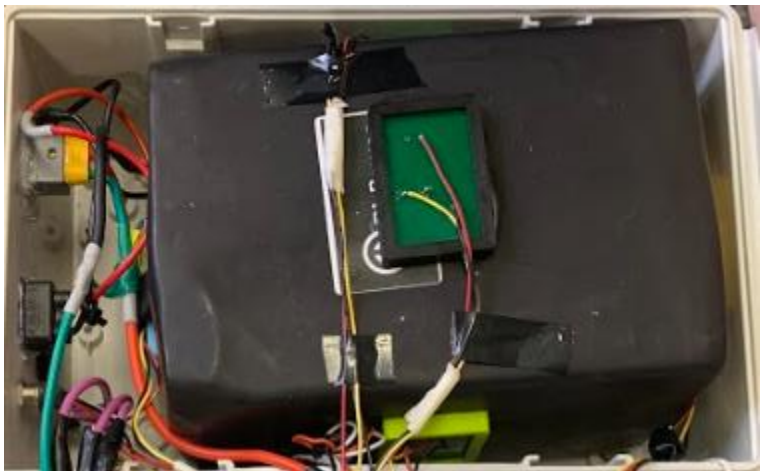

Figure 4.6.1 - Temperature Sensor Printed Circuit Board and Custom 3D Printed Case on Battery within Electronics case

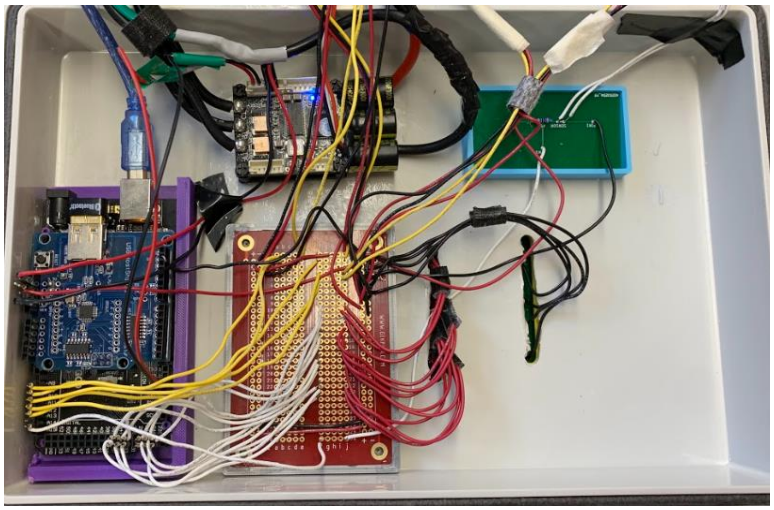

Figure 4.6.2 - Electronics Layout in Junction Box Lid

The LED notification PCB and 3D printed case were placed on the outside of the electronics box so that the LED notification system is visible to the rider. To integrate the LED notification board into the rest of the system, holes were drilled which lined up with the circuit board so that wires are protected as they are routed to the Arduino. The notification system circuit board is sealed within its case, which is sealed to the board to maintain the integrity of the waterproof box.

The complete wiring diagram is provided in appendix 6.D. The pressure sensor, temperature sensor and LED breadboard were all connected to a 5V and ground bus line and then the Arduino, this helped save space as the Arduino had limited 5V and ground pins. For simplicity, only one LED and temperature sensor was included in the wiring diagram. This also met the needs of the sensors as each operation 3.3-5V. Incorporating the electronics system into

the mechanical design of the system is simple. To power the motor, the protected motor power wires were routed through one of the sidewalls of the ground interface. To install the electrical system within the ground interface chassis, space was allotted between the axles of the driveline to allow for the wires to be routed through. The motor power wire is secured with zip ties along the back of the bindings and the arm mechanism of the drive system so that the cord does not interfere with regular use of the device.

Furthermore, the placement of the electronics system case was a factor in some of the mechanical design and calculations of the prototype. The battery itself has a mass of approximately 6.3 kg and the electronics system have a mass about 6.8 kg. By placing the electronics box in the center of the board, the rider's center of mass does not change. Originally, the team planned for the battery and electronics system to be housed within a backpack that the rider would have to carry. However, the electronics box is heavy, includes high current wires with no way to safely route them, and shifts the rider's center of mass potentially increasing balance difficulty. Thus, placing the box on the board between the bindings was the most ideal for the device.

5.0 Results

Mechanical testing of the device began during the design process, through simulations of various sections of the drive system, ground interface and suspension mechanism. Calculations and simulations were completed regarding the mechanical systems to ensure that all of the manufactured parts would function as expected and support the weight and movement of a rider during regular device use.

Individual system testing regarding electronics and software included first, setting up the Xbox controller, and integrating the circuits with the pressure sensor, temperature sensor and LEDs one at a time. Testing the Xbox controller confirmed the functionality of haptic feedback, and the controller's ability to communicate with the Arduino was verified with multicolored LEDs. Once the Xbox controller testing was completed, the Xbox controller was tested with the motor and pressure sensor, to ensure that the controller would vibrate, and the motor turn off when the rider is not strapped in correctly. The temperature sensors were tested prior to being incorporated with the full system, and temperatures were recorded from within a kitchen freezer and room temperature room. All readings were verified with the actual temperature of the environment the sensors were placed in. The notification system was the last integrated as the function of the LEDs is contingent on the rest of the sensors functioning properly. Following the testing of the pressure sensor, Xbox controller and temperature sensors, the notification system was verified by testing the individual system and ensuring the LEDs lit up per the correct input.

Full system testing was completed following the assembly of the entire prototype at Wachusett Mountain. Because testing occurred after the end of the skiing and snowboarding season, the snow available on the mountain was hard packed, and wet. This meant the team could not test the functionality of the arm suspension mechanism in multiple types of snow. The

team planned to test the device unloaded, loaded with small weights, and with a rider. Although the full device was only tested once, it was successfully able to push itself without any added weight. Unfortunately, the battery was not able to hold a sufficient charge to move the device without being plugged into a laptop, or additional battery. Moving forward, the team plans to replace the battery to ensure the full device works as expected. Despite this, the notification system, drive system and arm mechanism all behaved as expected.

6.0 Next Steps

Although the device was fully manufactured and assembled before the end of the academic term, there is room for improvement throughout all major subsystems. Regarding mechanical design, decreasing the overall weight would make turning easier for the rider, improve battery life and improve lift ability. For the electrical and software systems, consolidating electronics and simplifying the control scheme would reduce weight and streamline device maintenance. Further testing of the prototype is also necessary to determine the devices capabilities including battery life, overall durability and verify mechanical calculations.

Mechanical improvements to the device fall under two main categories, increasing maneuverability and better protection for the rider and device. An improvement to the maneuverability would be enabling the ground interface to rotate about both the board axis (roll) and the axis perpendicular to the earth's surface (yaw). Enabling rotation about both of these axes will facilitate turning as the rider would not need to rotate the ground interface along with the rest of the board. One idea for this is replacing the mechanical arms with flexible urethane arms that can bend about both roll and yaw axes. Also, a modern snowboard with better edges and a lighter build would allow the rider to cut into the snow and tilt the board more easily. Another way we would like to facilitate turning is to reduce the overall weight of the device by replacing some of the heavy metal parts with lighter plastics. If weight was reduced a stronger suspension would need to be designed to develop enough tractive effort. For protecting the rider, the current safety shroud is serviceable, but it could be improved as it was not thermoformed in an oven. The bends in the polycarbonate do not exactly match the designed curves, which prevents proper flipping of the ground interface for downhill action. After testing on snow, the gears had ice on them, to remedy this a more elaborate protective gearbox should be developed, as the current design only protects the driving gear and not the follower gear.

Regarding software and electrical improvements, the main goal is to simplify the system. The first step is replacing the Xbox controller with a custom remote. The Xbox controller was great for prototyping since it had many buttons and the vibration capability that was necessary for haptic feedback. However, an Xbox controller is designed for two hands, where we would like the rider to operate the device with a single hand, and only one button was used for speed control. Based on our research, there is not a controller that fits all design requirements, is within project budget and includes haptic feedback. Making a custom controller would also allow us to use a different communication protocol and not require the Arduino USB Host Shield. A custom

controller would have the buttons and layout more suited to our device and could fit within one hand.

Other than the remote, we would like to build a battery and case to accommodate internal thermal regulation. This was a part of our initial plans to ensure the battery was operating within its ideal temperature range. With temperature regulation, the rider could keep the device outside longer because they could operate the device entirely outside including charging the battery without risking damaging the battery. Also, this would ensure other PCBs and components that were also temperature sensitive would stay within their ideal operating temperature ranges. Unfortunately, due to the lack of space inside the container and time to develop the control system, we were not able to fit a thermal regulation system. Therefore, for future iterations, we would want to design and build a custom heat resistant case and battery pack for more accurate temperature monitoring and control.

Lastly, regarding software, the methods for monitoring the devices that were implemented were not ideal and require improvement in future project iterations. For motor stall detection, we plan to not shut off the motor when it stalls although we still want to alert the rider. For battery SOC estimation, we plan to implement a coulomb counting algorithm or purchase a battery capacity meter to provide more accurate estimates. In addition, we want to implement more energy saving features to improve battery life without needing a larger battery such as regenerative braking and solar panels. Technologies still in their infancy, such as thermoelectric, pyroelectric, and hydrogen fuel cell-based energy storage could also enable more efficient power usage.

Unfortunately, a functional full-scale prototype was not completed in the duration of the project. The team acknowledges that many of the goals that would have been confirmed by a full-scale prototype cannot be confirmed, but the team has narrowed down issues with the devices function to issues with the battery. Moving forward, a replacement battery should ensure a functional prototype and more robust thermal regulation system, as well as lighter mechanical parts and the other improvements in the section should improve on the prototype.

7.0 Appendix

7.A Contact Pressure Calculation from Snowshoes

Recommended Snowshoe Length vs. Rider Weight for Different Trail Conditions			
User Weight (kg)	**Packed Snow (cm)**	**Soft Snow (cm)**	**Soft & Deep Snow (cm)**
41-57	56	56	60
57-79	56	60	64
79-102	56	64	80
102+	64	76	91

Figure 7.A.1 - Snowshoe Length Chart, adapted from MSR Gear "Snowshoe Sizing: How to Pick your Perfect Length" [48]

Using an average of modern snowshoe width of 24 cm, a surface area can be calculated for each table value. Using the assumption that the "worst case" condition for flotation occurs in the least dense snow (i.e., "soft and deep snow" in the table), the weight to surface area ratios for each weight category were found.

User Weight Average (N)	**Snowshoe Area (m^2)**	**Contact Pressure (N/m^2)**	**Contact Pressure (lb/in^2)**
480	.144	3,330	.48
667	.154	4,330	.63
893	.192	4,650	.67
1050	.218	4,810	.70

Figure 7.A.2 - Calculation of Pressures for Snowshoe Flotation.

For a conservative analysis, the minimum pressure ratio (3,330 Pa) found in this table is used as the target. It is estimated that a pressure ratio of 3,330 Pa (0.48 psi) should be seen as the maximum pressure ratio of snow devices seeking to traverse "soft and deep snow" according to the snowshoe sizing table.

7.B Propulsion Design Preliminary Sketches

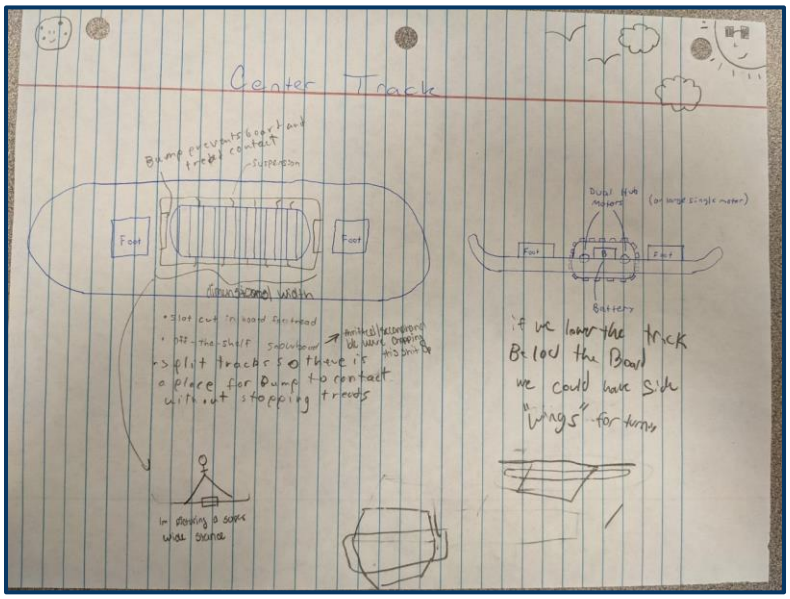

Figure 7.B.1 - Tracks

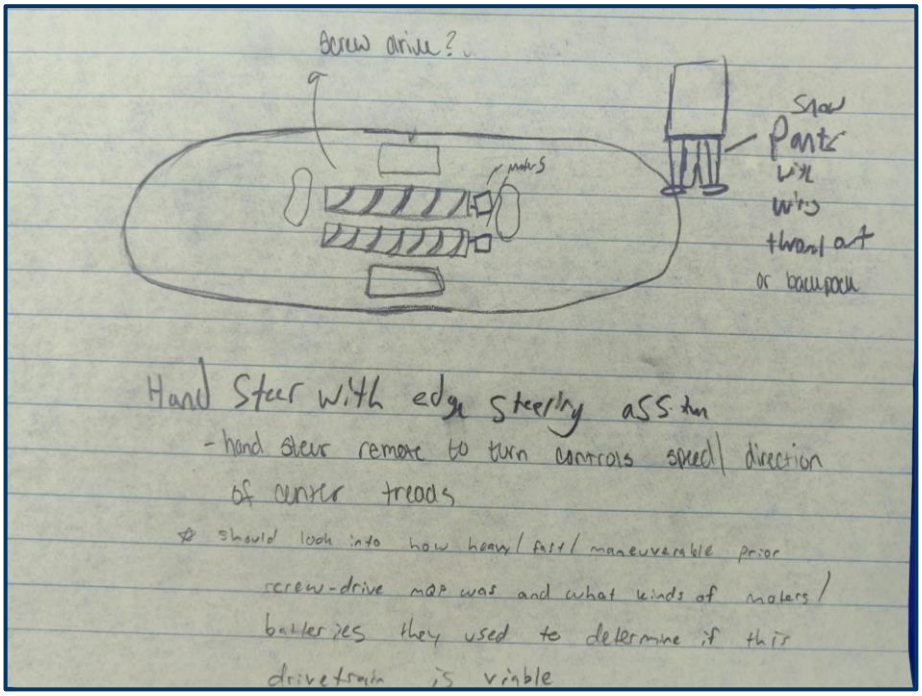

Figure 7.B.2 - Screw Drive

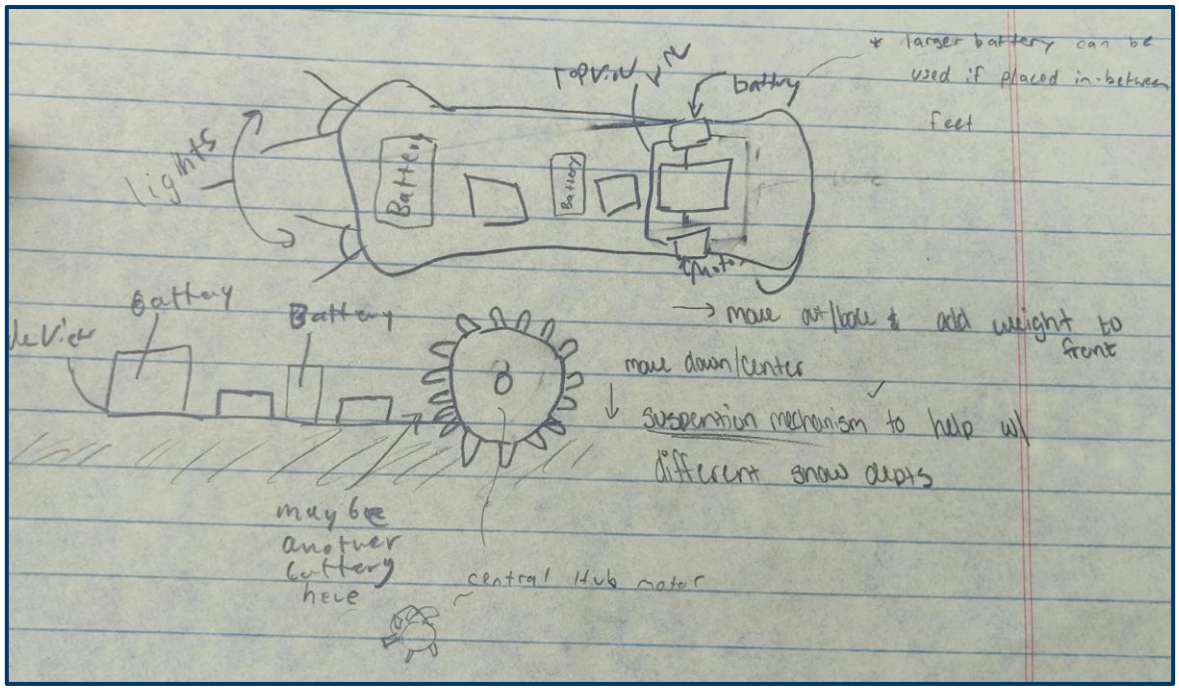

Figure 7.B.3 - Single Paddle Wheel

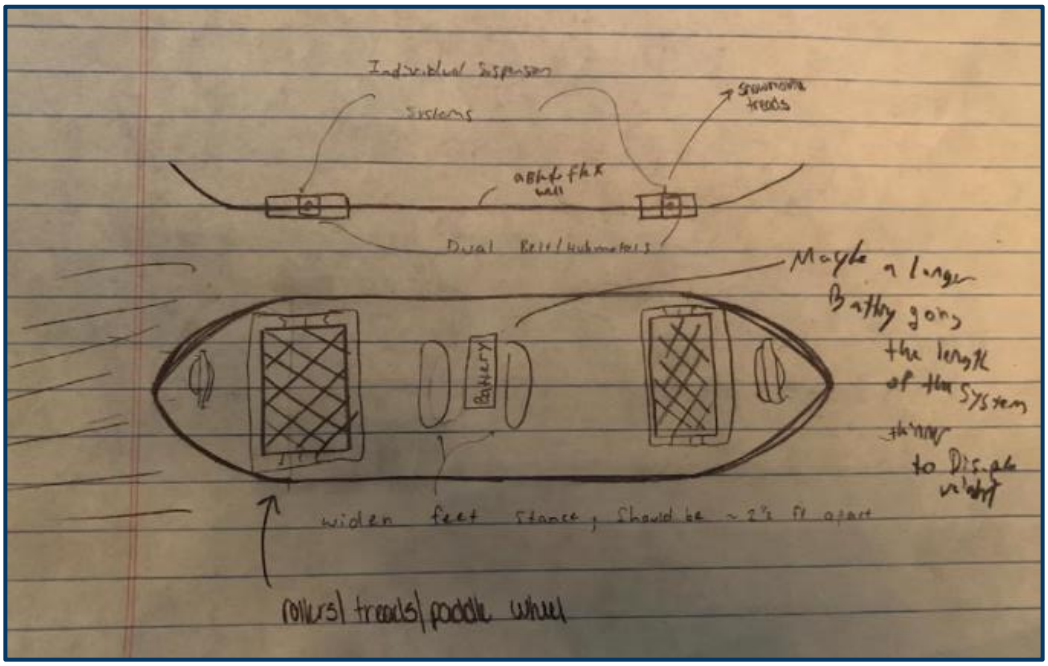

Figure 7.B.4 - Dual Paddle Wheel

7.C Software UML Diagram

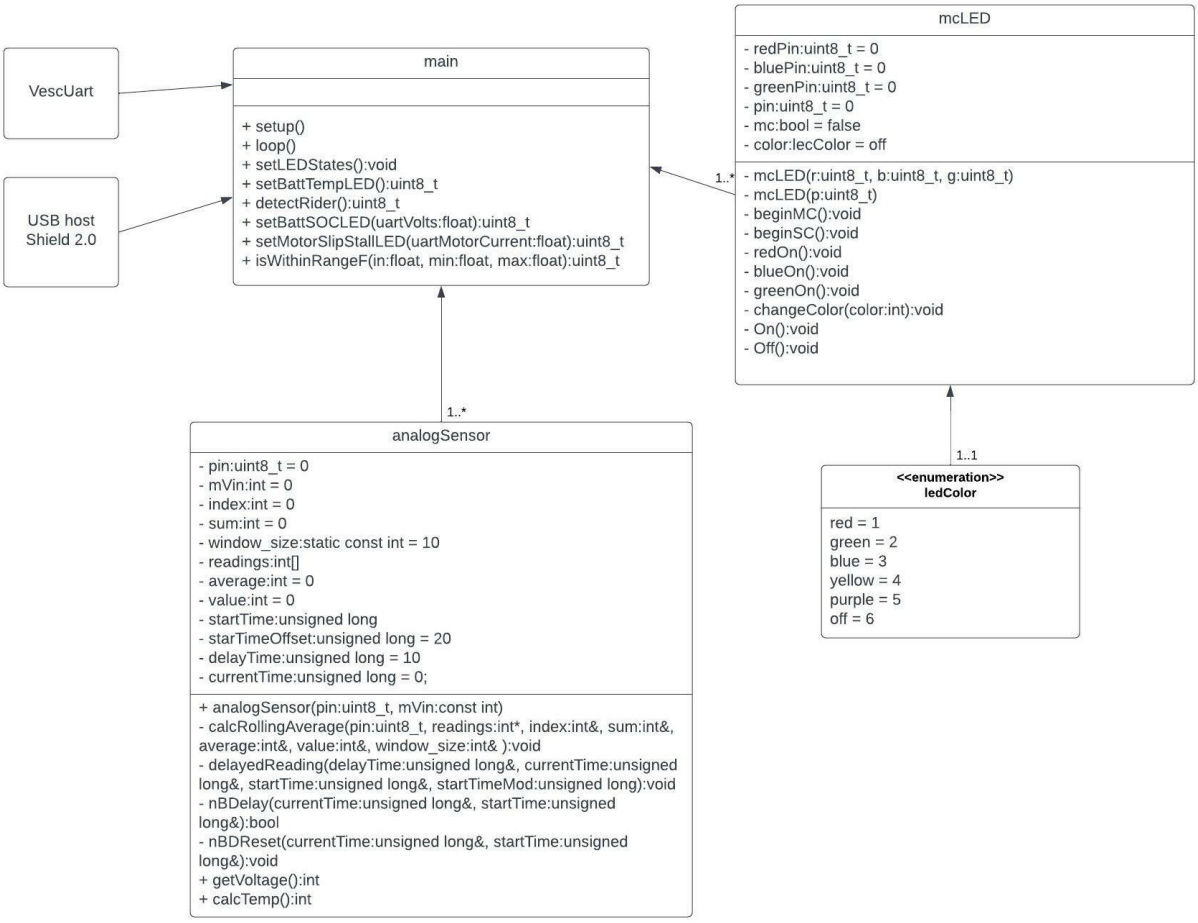

7.D Wiring Diagram

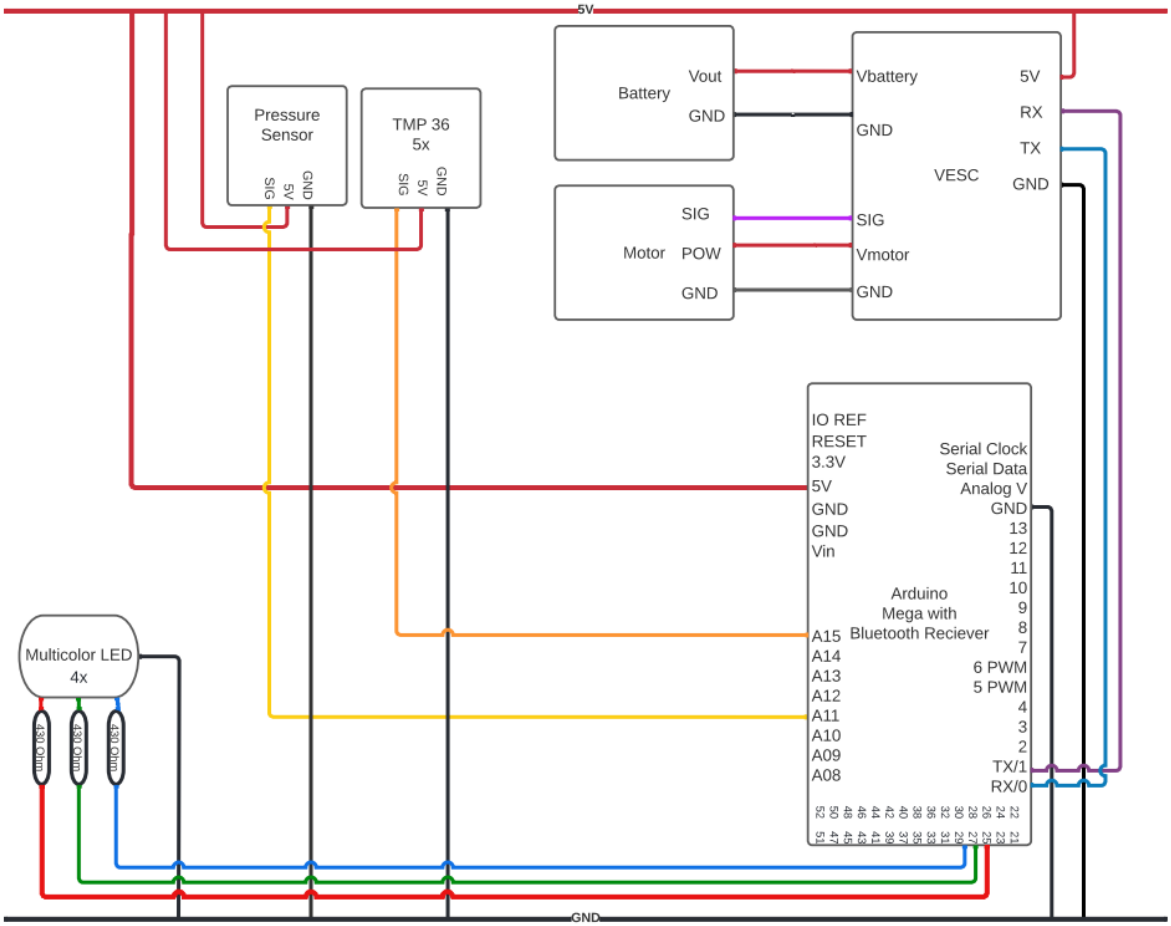

7.E Commercially Available Electric Skateboards used to Approximate Industry Standards

Board	**Source**
Meepo Hurricane	"Meepo hurricane," *Meepo Board*. [Online]. Available: https://www.meepoboard.com/products/meepo-hurricane?variant=39507693666398. [Accessed: 14-Oct-2021].
Backfire Ranger	"Backfire Ranger X2 all Terrain Electric skateboard with 1200W X2 ultra high power ultra high torque motors and 12s high voltage high efficiency electronic system," *Backfire Boards*. [Online]. Available: https://www.backfireboards.com/products/backfire-ranger-x2-all-terrain-electric-skateboard-with-1200w-x2-ultra-high-power-ultra-high-torque-motors-and-12s-high-voltage-high-efficiency-electronic-system. [Accessed: 14-Oct-2021].
WowGo AT2	"WowGo AT2 Electric Skateboard & Longboard," *WOWGO BOARD*. [Online]. Available: https://wowgoboard.com/products/wowgo-all-terrain-electric-skateboard. [Accessed: 14-Oct-2021].
Teamgee H20T	"Teamgee H20T electric skateboard with rubber wheels," *Teamgee Skateboard*. [Online]. Available: https://www.teamgee.com/products/teamgee-h20t-electric-skateboard-with-rubber-wheels. [Accessed: 14-Oct-2021].
Evolve Bamboo GTR AT	"Bamboo GTR all terrain," *Evolve Skateboards USA*. [Online]. Available: https://evolveskateboardsusa.com/products/gtr-bamboo-all-terrain. [Accessed: 14-Oct-2021].
Exway Atlas Carbon 2WD All Terrain	"Exway Atlas Carbon-2WD," *ExwayStore | The Most advanced Electric Skateboard*. [Online]. Available: https://www.exwayboard.com/products/exway-atlas-carbon-2wd. [Accessed: 14-Oct-2021].
Lacroix Navare Lonestar	"Nazaré Lonestar™," *Lacroix Boards*. [Online]. Available: https://lacroixboards.com/products/nazare-lonestar%E2%84%A2-new. [Accessed: 14-Oct-2021].
Bajaboard S2-Atrax	"Atrax: Bajaboard - extreme offroad E-board," *BajaBoard*. [Online]. Available: https://bajaboard.com.au/bajaboard-s2-atrax. [Accessed: 14-Oct-2021].
Radley Carbon V2 Off Road Electric Skateboard	"Raldey carbon at V.2 off-road electric skateboard," *Raldeyboards*. [Online]. Available: https://raldey.com/products/raldey-carbon-at-v2. [Accessed: 14-Oct-2021].
Metroboard X	"MetroboardX - all terrain + street electric skateboard," *Metroboard*, 17-Sep-2021. [Online]. Available: https://metro-board.com/e-skate-shop/all-terrain-electric-skateboard-metroboardx/. [Accessed: 14-Oct-2021].
AEBoards AT2	"Aeboard AT2 (all terrain)," *AEboard.* [Online]. Available: https://www.aeboarder.com/products/all-terrain-electric-skateboard-39-inch-aeboard-at2-at1-upgrade-version. [Accessed: 14-Oct-2021].

7.F Small Scale Prototyping

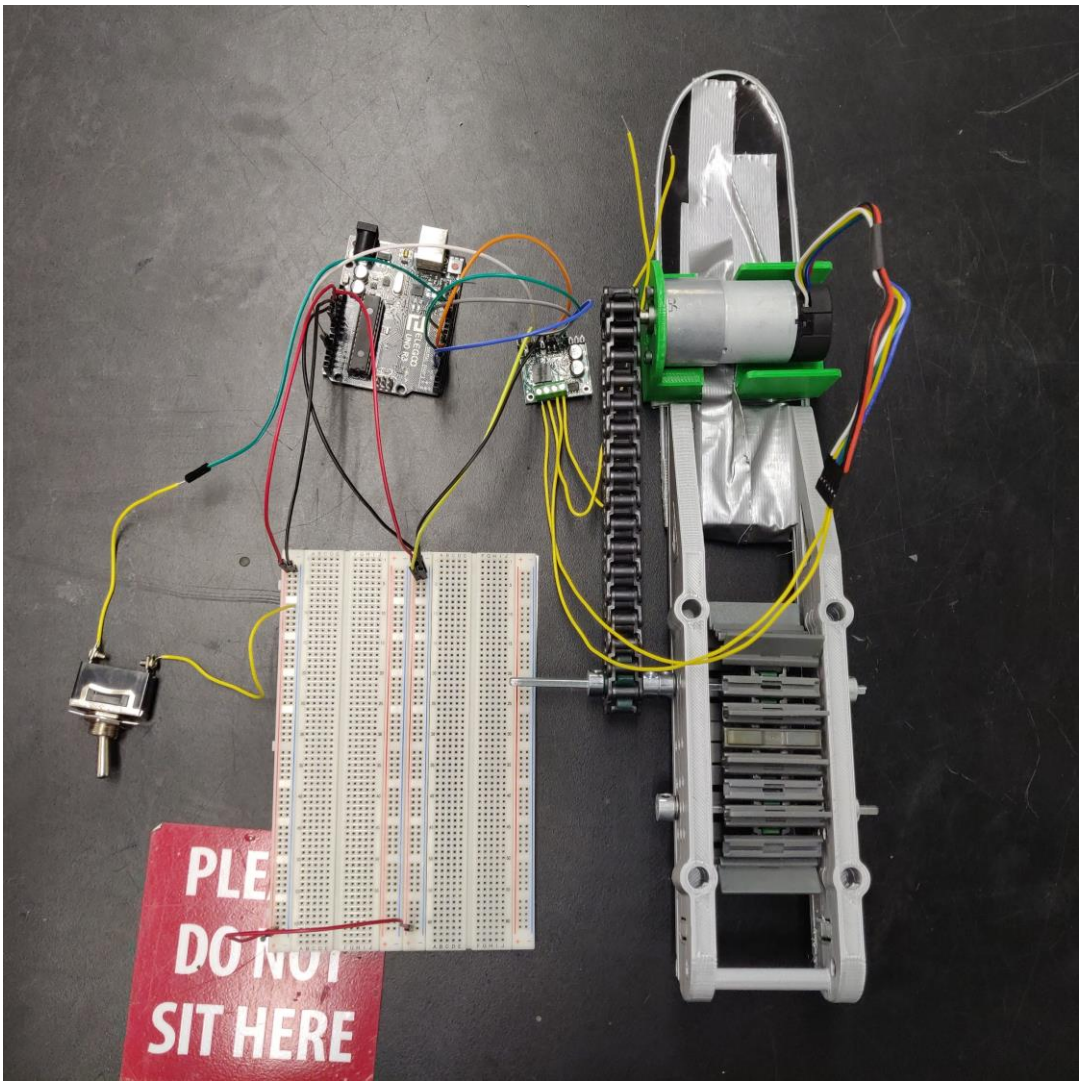

Full Assembly of Mini-Prototype with Small Grousers

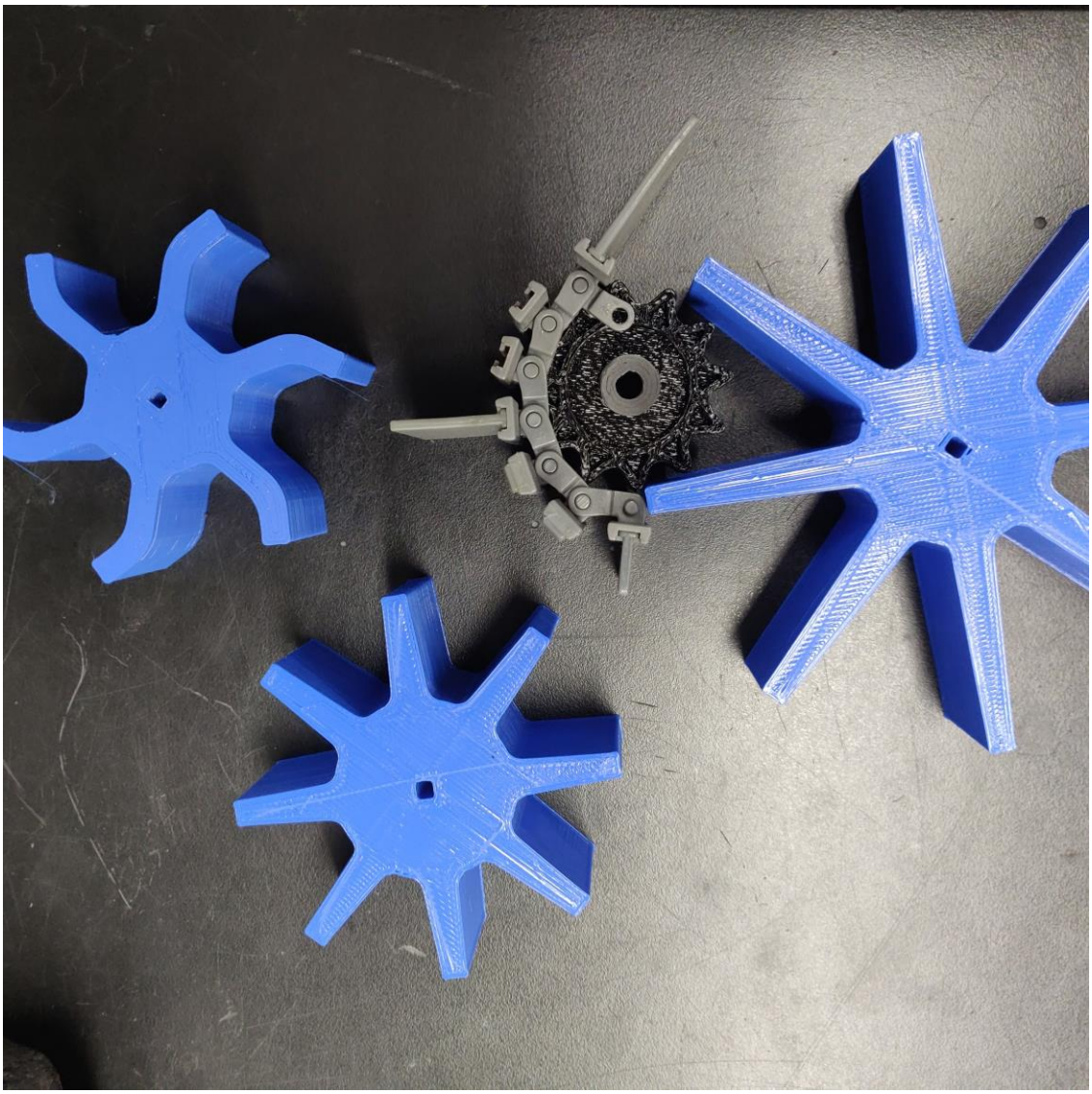

The Three Different Paddle wheels and the 3 Grocers

8.0 References

[1] S. L. Center, “Sherman Poppen's snurfer,” Lemelson Center for the Study of Invention and Innovation, 25-Nov-2019. [Online]. Available: https://invention.si.edu/sherman-poppen-s-snurfer. [Accessed: 14-Oct-2021].

[2] C. Louison, *Impossible: Rodney Mullen, Ryan Sheckler, and the fantastic history of skateboarding*. Oak Knoll, 2011.

[3] James Flynn May 14, “The history of Skateboarding & The Evolution of the Electric Skateboard,” *Transportation Evolved*, 14-May-2019. [Online]. Available: https://transportationevolved.com/history-of-skateboarding-electric-skateboard/. [Accessed: 14-Oct-2021].

[4] J. Y. Wong, *Theory of Ground Vehicles*. New York: John Wiley, 2001.

[5] M. G. Bekker, *Theory of Land Locomotion: The Mechanics of Vehicle Mobility*. Ann Arbor, 1956.

[6] Eskelson, Ross W., "A Comparison of Over-Snow Vehicles Produced at Utah State Agricultural College" (1955). All Graduate Theses and Dissertations. 968.

[7] Tatsuro, Muro, and Jonathan O’Brien. Terramechanics. Lisse, A.A. Balkema Publishers, 2005.

[8] T. Guo, “Power Consumption Models for Tracked and Wheeled Small Unmanned Ground Vehicles on Deformable Terrains,” dissertation, University of Michigan, Ann Arbor, MI, 2016.

[9] J. H. Lever, A. J. Delaney, L. E. Ray, E. Trautmann, L. A. Barna, and A. M. Burzynski, “Autonomous GPR surveys using the Polar Rover Yeti,” Journal of Field Robotics, vol. 30, no. 2, pp. 194–215, 2012.

[10] The Physics Factbook. 2021. Coefficients of Friction for Snow - The Physics Factbook. [online] Available at: <https://hypertextbook.com/facts/2007/TabraizRasul.shtml> [Accessed 7 October 2021].

[11] Lematta, C., 2014. Simple Beauty. [online] Physics of Snowboarding. Available at: <http://ffden-2.phys.uaf.edu/webproj/212_spring_2014/Craig_Lematta/craig_lematta/page1.html> [Accessed 7 October 2021].

[12] “Direct Shear Test,” *Geoengineer.org*. [Online]. Available: https://www.geoengineer.org/education/laboratory-testing/direct-shear-test. [Accessed:12-Oct-2021].

[13] S. Poppen , “Surf-Type Snow Ski” U.S. Patent 3,378,274, Mar 17, 1966

[14] F. Normani, The Physics Of Snowboarding, Available: https://www.real-world-physics-problems.com/physics-of-snowboarding.html

[15] Donek Snowboards “A physics lesson about Snowboard turn shape: Part 1” Y*ouTube*, Aug. 22, 2011. [Video recording]. Available: https://www.youtube.com/watch?v=uE1YdDj_L0o

[16] C. Debresson and N. Baker “Snowmobiles in Canada” in *The Canadian Encyclopedia* Dec 3, 2020. [Online] Available: https://www.thecanadianencyclopedia.ca/en/article/snowmobile#

[17] *Nomad Utility* Taiga Motors Corporation, 2021.[Online] Available: https://taigamotors.ca/snowmobiles/

[18] *Powerboard* Mattracks Inc.[Online] Available: https://www.mattrackspowerboards.com/

[19] The Green Head *Mattracks Powerboard - Gas-Powered Motorized Snowboard* Ominea December 1, 2008. [Online] Available: https://www.thegreenhead.com/2008/12/mattracks-powerboard-gas-powered-motorized-snowboard.php

[20] powertraverse *[@powertraverse]* “First production batteries arrived…” Instagram May 13, 2021.[Online]Available: https://www.instagram.com/p/CO0QYRLsVKP/

[21] *The Skizee Woodrunner.* Skiee Canada [Online]. Available: https://skizee.ca/

[22] Hacksmith Industries “ ELECTRIC Snowboard goes TOO FAST!” *Youtube,* Feb 19, 2018. [Video recording]. Available: https://www.youtube.com/watch?v=MnLMvYeJABA

[23] Hacksmith Industries “JET ENGINE Powered Snowboard! (ONE DAY BUILD)” *Youtube,* Jan 28, 2021. [Video recording]. Available: https://www.youtube.com/watch?v=BCBk_KWoauI

[24] *Design* Propel~Surf.[Online] Available: http://www.propulsurf.com/home.html

[25] SnoDeck “SnoDeck” *Youtube,* Mar 29, 2007. [Video recording]. Available: https://www.youtube.com/watch?v=WYxhoUqL8F4

[26] *Augerboard Or Auger In Miniature* НПО «Карманный транспорт» [Online] Available: https://www-motocamokat-ru.translate.goog/shnekosnoubord_ili_shnekohod_v_mini?_x_tr_sl=ru&_x_tr_tl=en&_x_tr_hl=en&_x_tr_pto=nui,sc&_x_tr_sch=http

[27] Homemade Mehanol "Home made Electric snowboard " *Youtube,* Dec 16, 2017. [Video recording]. Available: https://www.youtube.com/watch?v=pEPyi8m_V5w

[28] *What does Cold Cranking Amps (CCA) mean?* Optima Batteries [Online] Available: https://www.optimabatteries.com/experience/blog/what-does-cold-cranking-amps-(cca)-mean

[29]*Differences Between Brushed and Brushless DC motors*. YouTube, 2015.

[30] "Motor operation in hot and cold climates," *WorldWide Electric*, 12-Jan-2021. [Online]. Available: https://www.worldwideelectric.net/articles/motor-operation-hot-cold-climates/. [Accessed: 08-Oct-2021].

[31] "4 tips for using an electric motor during the winter months," *Groschopp*, 23-Apr-2018. [Online]. Available: https://www.groschopp.com/4-tips-for-using-an-electric-motor-during-the-winter-months/. [Accessed: 08-Oct-2021].

[32]Frank, "5. additional settings: Throttle Curves, ERPM limits, safety features etc..," 5. Additional settings: Throttle curves, ERPM limits, safety features etc. | VESC Project, 03-Oct-2017. [Online]. Available: https://vesc-project.com/node/183. [Accessed: 08-Oct-2021].

[33]E. Jacobsen, "VescUART," VescUart library for interfacing Arduino with VESC. Github.

[34]P. Lim, "Understanding ESC & VESC in electric skateboard: How to choose?," Electric Skateboard HQ, 29-Nov-2019. [Online]. Available: https://www.electricskateboardhq.com/understanding-electronic-speed-controller-esc-and-vesc/. [Accessed: 08-Oct-2021].

[35] "How to choose ESC for Quadcopter: Electronic Speed Controller," *Drone Nodes*. [Online]. Available: https://dronenodes.com/drone-esc-electronic-speed-controller/. [Accessed: 13-Oct-2021].

[36]VESC Team, "VESC Tool," VESC project. [Online]. Available: https://vesc-project.com/vesc_tool. [Accessed: 08-Oct-2021].

[37]C. Saad, B. Mostafa, E. Ahmadi, and H. Abderrahmane, “Comparative Performance Analysis of Wireless Communication Protocols for Intelligent Sensors and Their Applications,” IJACSA, vol. 5, no. 4, 2014, doi: 10.14569/IJACSA.2014.050413.

[38]S. Al-Sarawi, M. Anbar, K. Alieyan, and M. Alzubaidi, “Internet of Things (IoT) communication protocols: Review,” in 2017 8th International Conference on Information Technology (ICIT), Amman, Jordan, May 2017, pp. 685–690. doi: 10.1109/ICITECH.2017.8079928.

[39]M. Siekkinen, M. Hiienkari, J. K. Nurminen, and J. Nieminen, “How low energy is bluetooth low energy? Comparative measurements with ZigBee/802.15.4,” in 2012 IEEE Wireless Communications and Networking Conference Workshops (WCNCW), Paris, France, Apr. 2012, pp. 232–237. doi: 10.1109/WCNCW.2012.6215496.

[40]Last Minute Engineers, “In-depth: How NRF24L01 wireless module works & interface with Arduino,” *Last Minute Engineers*, 18-Dec-2020. [Online]. Available: https://lastminuteengineers.com/nrf24l01-arduino-wireless-communication/. [Accessed: 08-Oct-2021].

[41]“nRF24L01+ Single Chip 2.4GHz Transciever.”

[42]T. Waters, V. Puts-Anderson, and A. Garg, “NIOSH math model for lifting weights.pdf.” US Department of Health and Human Services, Jan. 1994.

[43] “Loud noise dangers,” *American Speech-Language-Hearing Association*. [Online]. Available: https://www.asha.org/public/hearing/loud-noise-dangers/#:~:text=If%20the%20sound%20goes%20up,is%20down%20to%202%20hours. [Accessed: 08-Oct-2021].

[44] C. Thompson, “What are Good Ski Conditions?,” SportsRec, 15-Oct-2019. [Online]. Available: https://www.sportsrec.com/6665987/what-are-good-ski-conditions. [Accessed: 05-Oct-2021].

[45] M. Shapiro, M. S. J. 14, M. S. J. 15, and M. S. J. 12, “3 effective ways to simulate hiking on a treadmill,” *Fit For Trips*, 21-Feb-2021. [Online]. Available: https://fitfortrips.com/how-to-simulate-hiking-on-a-treadmill/. [Accessed: 08-Oct-2021].

[46]J. Holmes, “How much does a snowboard weigh with 8 examples,” Crowsurvival, 19-Nov-2020. [Online]. Available: https://crowsurvival.com/how-much-does-a-snowboard-weigh/. [Accessed: 08-Oct-2021].

[47]“How much do snowboards weigh? (explained),” OutdoorAlive, 03-Aug-2021. [Online]. Available: https://outdooralive.com/how-much-snowboards-weigh/. [Accessed: 08-Oct-2021].

[48] MSR Team, “Snowshoe sizing: How to pick your perfect length ,” *The Summit Register*, 07-Jan-2021. [Online]. Available: https://www.msrgear.com/blog/snowshoe-sizing-how-to-pick-snowshoe-length/. [Accessed: 08-Oct-2021].

[49] “IP Rating Chart,” *DSM&T*. [Online]. Available: https://www.dsmt.com/resources/ip-rating-chart/. [Accessed: 14-Oct-2021].

[50] “Past and Present of LiFePO4: Forms Fundamental Research to Industrial Applications” Available: https://www.sciencedirect.com/science/article/pii/S2451929418305758

[51] “Northeast Battery: The Region's Largest Independent Battery Distributor” Available: https://northeastbattery.com/

[52] “Batteries Unlimited” Available: https://www.batteriesunlim.com/

[53] “BtrPower Electric Bike Battery 20AH 36v 48v 60v 72v LiFePO4 Battery Pack with 50A BMS and 5A Fast Charger for 1500W-350W Motor, Perfect for EBike E-Scooter E-Tricycle E-Motorcycle” Available: https://www.amazon.com/BtrPower-Battery-Lithium-Lifepo4-Electric

[54] QILIPSU Hinged Cover Stainless Steel Latch 300x200x170mm Junction Box with Mounting Plate, Universal IP67 Project Box Waterproof DIY Electrical Enclosure, ABS Plastic Grey (11.8"x7.9"x6.7")
https://www.amazon.com/dp/B096X82P1L?ref=ppx_yo2ov_dt_b_product_details&th=1

[55] TMP36 Temperature Sensor Available: https://learn.adafruit.com/tmp36-temperature-sensor

[56] BU-903: How to Measure State-of-charge
Available: https://batteryuniversity.com/article/bu-903-how-to-measure-state-of-charge

[57] “Gears and gearing stress and selection - Mercer university.” [Online]. Available: http://faculty.mercer.edu/jenkins_he/documents/Gears4StressandSelection.pdf. [Accessed: 26-Apr-2022].

[58] S. Ma et al., “Temperature effect and thermal impact in lithium-ion batteries: A review,” Progress in Natural Science: Materials International, vol. 28, no. 6, pp. 653–666, Dec. 2018, doi: 10.1016/j.pnsc.2018.11.002.

[59] Arduino Nano Available: https://store-usa.arduino.cc/products/arduino-nano?selectedStore=us

[60] Lady Ada, “Current Draw” Available: https://learn.adafruit.com/rgb-led-strips/current-draw

[61] “Pulley & Keyway & Belt,” *FLIPSKY*. Available: https://flipsky.net/collections/pulley.